UNIVERSITÀ DEGLI STUDI DI PADOVA

"Galileo Galilei", Physics and Astronomy Department

M.Sc. Physics

Master's thesis

The eigenstate thermalisation hypothesis and the quantum many-body scars

Supervisors

Prof. Simone MONTANGERO

Prof. Leonardo MAZZA

Candidate

Gianluca MORETTINI

A.Y. 2022/2023

Abstract

The Eigenstate thermalization hypothesis (ETH) represents the current most developed framework to explain the onset of thermalization in isolated many-body quantum systems. In this thesis we will focus on quantum many-body scars, and in particular on their asymptotic version. Quantum many-body scars are notoriously associated to a non-ergodic dynamics and to relaxation times that diverge in the thermodynamic limit; briefly, these states fail to thermalize. The goal of this thesis is to investigate the violation of ETH associated to asymptotic quantum many-body scars.

Contents

List of Figures

List of Tables

Introduction

Thermalization, the process through which a physical system reaches equilibrium and exhibits macroscopic behaviour consistent with the laws of thermodynamics, has intrigued scientists for centuries. Despite the remarkable success of statistical mechanics in describing the macroscopic properties of systems, the fundamental connection with microscopic dynamics remains a subject of ongoing investigation and debate. This is true for quantum and classical systems.

To introduce the problem, let us consider a classical example. Imagine a Becher filled with water, where a drop of colourant is added at a specific time. As time progresses, one can expect that the system will reach an equilibrium, the colourant is spread in the entire liquid. The thesis investigates the behaviour of quantum systems in comparison to classical mechanics. The work aims to examine whether a quantum system exhibits similar behaviour.

Remarkably, the recent Eigenstate thermalization hypothesis (ETH) has put the problem of understanding thermalization in quantum systems on more solid foundations. This hypothesis is devoted to unravelling the mechanisms underlying the temporal evolution of systems initially prepared in states markedly distant from equilibrium, eventually transforming into states that conform to the framework of thermal equilibrium [1].
ETH combines ideas of chaos and typical configurations in a clear mathematical form that is unparalleled in classical systems and enables us to predict how observables behave when the system is left to evolve.
The ETH establishes a robust correspondence between the microcanonical predictions about observables and the protracted temporal behaviours exhibited by their corresponding matrix elements. This nexus engenders a profound linkage that connects the statistical attributes of observables in conditions of equilibrium with their behaviours during temporal evolution.
Numerical evidence of the occurrence of Eigenstate thermalization has been found in several strongly correlated nonintegrable lattice models in fields ranging from condensed matter to ultracold quantum gases. Such evidence was first reported for a two-dimensional system of hard-core bosons and interacting spin chains, spinless and spinful fermions, soft-core bosons and the transverse field Ising model in two

dimensions [2–6].

However, within the domain of quantum many-body systems, instances arise wherein certain behaviours manifest deviance from the predictions set forth by the ETH. In these particular circumstances, discernible discrepancies give rise to states referred to as scars. When a many-body system is prepared within one of these states, its subsequent dynamics veer conspicuously away from thermal behaviour. Most of the present interest in quantum many-body scars (QMBS) originates from an experiment on a chain of interacting Rydberg atoms, in which the authors observed unexpected non-thermal behaviours when the array of atoms was prepared in a particular initial state [7].
The non-thermal features of which we are mentioning may be broadly classified [8]:

1. The existence of certain species of infinitely long-lived quasiparticles;

2. Persistent many-body revivals at finite times in the dynamics;

3. Non-thermal stationary states that have atypically low entanglement.

All of these points signal an absence of thermalization, touching on different aspects of the phenomenon. We stress that these non-thermal features are found in particular states sprinkled throughout the many-body spectrum, and these unique states coexist with typical thermal states at the same energy densities. The nomenclature of scarring has variously been used in the literature to signify the presence of any of the above features, or of all three at the same time [9].

Up to now, we have spoken of eigenstates which violate ETH. However, there exist states that are a particular combination of eigenstates of Hamiltonian that follow singularly the ETH predictions, that seem to behave as a quantum many-body scar (QMBS) [10]. They have an energy variance that goes to zero in the thermodynamic limit and asymptotically display the typical dynamical phenomenology of a QMBS, i.e. the lack of thermalization; hence we refer to such states as asymptotic QMBS (AQMBS).
These states possess the potential to illuminate novel categories of ETH violations, consequently forging a novel avenue to comprehend our initial inquiry: the investigation of quantum many-body system thermalization. These emergent states will serve as the central focus, forming the nucleus for the original contributions presented within this thesis.

In this thesis, our investigation unfolds across distinct sections, each unravelling a facet of quantum phenomena. We embark on our discussion by delving into the Eigenstate thermalization hypothesis and the realm of scar states in Chap. 1 and Chap. 2. Subsequently, our focus shifts to a compelling case study within a

spin-1 XY chain, meticulously introduced and discussed in Chap. 3. Within this captivating system, we encounter scars and the enigmatic asymptotic quantum many-body scar states (AQMBS). The subsequent sections harbour our original contributions. Chap. 4 scrutinizes the intricate relationship between the ETH and AQMBS, particularly concerning their slow dynamics. In conclusion, Chap. 5, we expound upon the process of crafting states that mirror the attributes of AQMBS through the transformation of thermal states. As such, this thesis introduces novel contributions that augment the ongoing advancement of our comprehension concerning quantum systems and their intricate behaviours.

Chapter 1

Eigenstate thermalization hypothesis

In the following chapter, we shall provide a short description of the fundamental principles encompassing chaos and Random Matrix Theory (RMT). These concepts stand as pivotal underpinnings of the Eigenstate thermalization hypothesis (ETH). The latter constitutes the principal statistical proposition within the paradigm of the thermalization problem.

1.1 Chaos in Physics

The concept of chaos started with the discovery of differential calculus applied to classical physics.
In this mathematical framework, a deterministic system is a system whose present state is in principle fully determined by its initial conditions, in contrast to a stochastic system. For a stochastic system, the initial conditions determine the future only partially, due to noise or other external circumstances beyond our control: the present state reflects the past initial conditions plus the particular realization of the noise encountered along the way.
A deterministic system with sufficiently complicated dynamics can fool us into regarding it as a stochastic one; disentangling the deterministic from the stochastic is the main challenge in many real-life settings, from stock markets to palpitations of chicken hearts. So, what is "chaos"?
In a game of pinball, any two trajectories $x(t)$ that start out very close to each other separate exponentially with time, and in a finite number of bounces, their separation $\delta x(t)$ attains the magnitude of L, the characteristic linear extent of the whole system. This property of sensitivity to initial conditions can be quantified

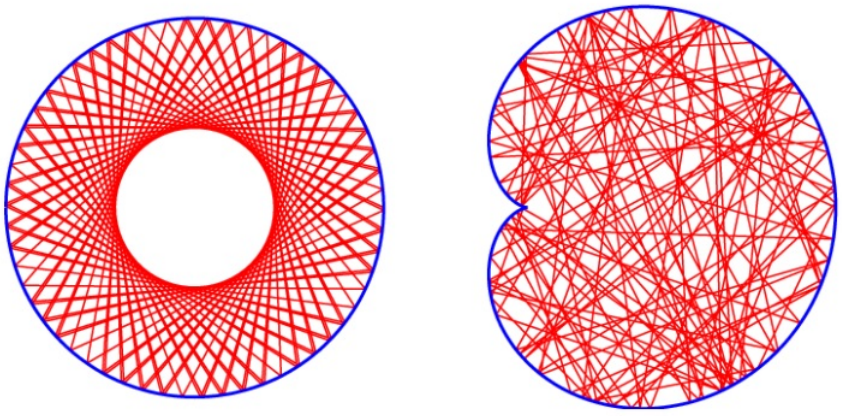

Figure 1.1: Trajectories in a circular billiard and a stadium billiard. The motion in the circle is regular or ordered, while in the stadium it is irregular or chaotic [13].

as

$$|\delta x(t)| \approx e^{\lambda t}|\delta x(0)| \tag{1.1}$$

where λ, the mean rate of separation of trajectories of the system, is called the Lyapunov exponent. For any finite accuracy $\delta x = |\delta x(0)|$ of the initial data, the dynamics is predictable only up to a finite Lyapunov time

$$T_{\text{Lyap}} \approx -\frac{1}{\lambda} \ln \left| \frac{\delta x}{L} \right| . \tag{1.2}$$

A positive Lyapunov exponent does not in itself lead to chaos [11, 12]. One could try to play a 1- or 2-disk pinball game, but it would not be much of a game; trajectories would only separate, never to meet again. What is also needed is mixing, the coming together again and again of trajectories. While locally the nearby trajectories separate, the interesting dynamics is confined to a globally finite region of the state space, and thus the separated trajectories are necessarily folded back and can re-approach each other arbitrarily closely, infinitely many times, as depicted in Fig. 1.1. In a general context, the enumeration of unique trajectories involving a specific number n of bounces, respecting the boundaries where the dynamics happens (in the considered case, the boundaries of the pinball), can be precisely characterized as follows:

$$N(n) \approx e^{hn} \tag{1.3}$$

where h, the growth rate of the number of topologically distinct trajectories, is called the topological entropy [11].

When a physicist designates a particular system as exhibiting chaos, the implication is that the system adheres to deterministic laws of evolution, albeit the outcome is exceedingly susceptible to minute uncertainties in the specification of the initial state. Within this context, the term chaos has adopted a specialized technical significance. If a deterministic system demonstrates local instability (positive Lyapunov exponent) and global mixing (positive entropy) it is characterized as chaotic [11, 14].
Although the definition of chaos as "positive Lyapunov exponent + positive entropy" is correct from a mathematical standpoint, its practical utility is limited, given that the quantification of these attributes is inherently asymptotic and remains elusive for systems observed in natural contexts. More potent is the characterization of chaotic behaviour through the phenomenon of the disappearance of invariant tori in the phase space. The concept of invariant torus necessitates a discussion on what is the nature of an integrable system.

Specifically, let a classical system whose Hamiltonian is $H(p, q)$, with canonical coordinates $q = (q_1, \ldots, q_N)$ and momenta $p = (p_1, \ldots, p_N)$, it is said to be integrable if it has as many functionally independent conserved quantities $I = (I_1, \ldots, I_N)$ as degrees of freedom N:

$$\{I_j, H\} = 0, \quad \{I_j, I_k\} = 0, \quad \text{where} \quad \{f, g\} = \sum_{j=1}^{N} \left(\frac{\partial f}{\partial q_j} \frac{\partial g}{\partial p_j} - \frac{\partial f}{\partial p_j} \frac{\partial g}{\partial q_j} \right). \quad (1.4)$$

From Liouville's integrability theorem [15], it follows that there is a canonical transformation $(p, q) \to (I, \Theta)$ (where I, Θ are termed action-angle variables) such that $H(p, q) = H(I)$ [16]. Consequently, the solutions of the equations of motion for the action-angle variables are trivial: $I_j(t) = I_j^0$ is constant, and $\Theta_j(t) = \Omega_j t + \Theta_j(0)$. This motion transpires on an N-dimensional torus, and it exhibits non-chaotic behaviour [17].
Consequently, within a non-integrable system, thus a system characterized by chaos, the count of functionally independent quantities must be less than the tally of degrees of freedom. In such a scenario, the feasibility of mapping the system's dynamics onto invariant tori is negated.

Now the question emerges naturally: how can we quantify chaos within the system? As previously discussed, a pronounced manifestation of chaos within classical systems is intrinsically interwoven with the intricacies of the phase space and how the dynamics spread over the phase space. In the realm of classical chaotic systems, a fundamental measure of chaoticity comes up: the Kolmogorov-Sinai entropy (KSE).
The Kolmogorov-Sinai entropy is established through an observation of a general nature. Specifically, γ exponential terms, presented in the form $e^{\lambda_i t}$, where λ_i is a Lyapunov exponent of the system, each possessing non-negative values, contribute

to the expansion of the separation between points residing within the phase space. In this context, the Kolmogorov-Sinai entropy is defined as [18]:

$$\Lambda_{KS} = \frac{1}{\gamma} \sum_{i=1}^{\gamma} \lambda_i. \tag{1.5}$$

Thus, the Kolmogorov-Sinai entropy decisively encapsulates the rate at which volumes of regions within the phase space undergo propagation.
One could measure this propagation or delocalization with the differently defined entropy [1]:

$$S_A = -\frac{1}{(2\pi\hbar)^D} \int dx\, dp\, \rho_A(x,p) \ln[\rho_A(x,p)], \tag{1.6}$$

where D is the dimensionality of the phase space and $\rho_A(x,p)$, is the classical reduced probability distribution (we are considering only the distribution N_A particles), obtained by averaging over the positions and momenta of the remaining $N - N_A$ particles:

$$\begin{aligned} &\rho_A(x_1, \ldots, x_{N_A}, p_1, \ldots, p_{N_A}, t) = \\ &\quad = \int dx_{N_A+1}\, dp_{N_A+1} \ldots\, dx_N\, dp_N\, \rho(x_1, \ldots, x_N, p_1, \ldots, p_N, t). \end{aligned} \tag{1.7}$$

It is important to note that the entropy S_A is expected to increase in time to the maximum value given by the Gibbs distribution

$$p(E) = \frac{1}{Z} e^{-\frac{E}{k_b T}} \tag{1.8}$$

where k_B is the Boltzmann constant, E and T are the energy and the temperature of the state achieved and Z is the partition function of the system.

In quantum systems, the situation is very similar. One can treat quantum chaos on the same footing as classical chaos analysing the delocalization of the system in the phase space. In particular, to measure the quantum chaos we redefine the probability distribution with a density matrix $\hat{\rho}$ in Eq. 1.6. More in detail, here, for subsystem A, we define the Von Neumann entropy:

$$S_{VN}^A = -\mathrm{Tr}_A \left[\hat{\rho}_A \ln \hat{\rho}_A\right], \tag{1.9}$$

where:

$$\hat{\rho}_A = \mathrm{Tr}_B[\hat{\rho}] \tag{1.10}$$

is the reduced density matrix.
We will focus on the case where S_{VN}^A have $\hat{\rho} = |\psi\rangle\langle\psi|$ and the subsystem A half of the total system. We call this bipartition entanglement entropy.

Alternatively, another avenue to gauge quantum delocalization lies in investigating the density matrix within the energy space. In the absence of degeneracies, the off-diagonal elements of the density matrix in the Hamiltonian's basis follow:

$$\rho_{mn}(t) = \rho_{mn}(t_0)e^{-i(E_m-E_n)(t-t_0)} \tag{1.11}$$

Therefore, time averaging:

$$\hat{\rho}_{\mathrm{DE}} \equiv \bar{\rho} \equiv \lim_{t_0\to\infty} \frac{1}{t_0}\int_0^{t_0} \hat{\rho}(t)dt = \sum_m \rho_{mm}|m\rangle\langle m| \tag{1.12}$$

constituting the diagonal subspace of the Hamiltonian, commonly referred to as the diagonal ensemble. This perspective establishes a linkage between the energy space and the phase space in the long-time regime.
Consequently, delving into the quantum system's delocalization in the phase space over extended temporal scales equates to probing the propagation of the initial density matrix within the spectrum of the Hamiltonian's eigenstates. In essence, this equates to exploration in the energy space [1].
The implications of investigating chaos through the energy space will be particularly noteworthy as we delve into the principal consequences arising from the ETH in Sec. 1.3.1.

1.2 Random Matrix theory

Quantum chaos is founded upon a pivotal array of outcomes, the bedrock of which is rooted in the fundamental endeavours of physicists such as Wigner, Dyson, and their contemporaries. Their endeavours culminated in the establishment of a comprehensive framework for understanding the spectral characteristics of intricate atomic nuclei. This seminal framework is known as Random matrix theory (RMT).
Central to the realm of quantum chaos is the profound capacity to scrutinize quantum energy levels. The examination of their statistical behaviour is in connection with the RMT. Among the principal facets engendered by this theory, the statistical attributes of level spacings (Level Spacing Statistics, LSS) take on a paramount significance. This junction of quantum chaos and the RMT has endowed the realm of physics with a profound toolset for unravelling the intricate dynamics of quantum systems characterized by chaotic dynamics.

Let us consider, for the sake of simplicity, a Hamiltonian $\hat{H} = \hat{H}_0 + \epsilon\hat{H}_1$ that comprises an integrable component $\hat{H}_0$ and a perturbing component $\hat{H}_1$ governed by a solitary parameter ϵ. Our investigation pertains to the manner in which

the energy levels of this Hamiltonian respond to variations in the perturbation parameter. Typically, when ϵ assumes small values, energy levels may intersect, yet as ϵ intensifies, a phenomenon emerges wherein the levels exhibit a propensity to "repel" each other. This phenomenon, known as level repulsion, constitutes an intrinsic attribute of non-integrable systems [19, 20]. A breif, albeit non-rigorous, elucidation of this phenomenon follows.

In particular, we consider a 2×2 Hamiltonian:

$$\hat{H} = \hat{H}_0 + \epsilon \hat{H}_1 = \begin{pmatrix} E_1 & 0 \\ 0 & E_2 \end{pmatrix} + \begin{pmatrix} 0 & H_{12} \\ H_{12}^* & 0 \end{pmatrix} = \begin{pmatrix} E_1 & H_{12} \\ H_{12}^* & E_2 \end{pmatrix} \tag{1.13}$$

where $H_{12} \propto \epsilon$, and E_1 and E_2 are the eigenvalues of the unperturbed Hamiltonian $\hat{H}_0$. The eigenvalues of $\hat{H}$ are expressed as:

$$E\pm = \frac{1}{2}(E_1 + E_2) \pm \sqrt{\frac{(E_1 - E_2)^2}{4} + |H_{12}|^2}. \tag{1.14}$$

Upon defining $\Delta E = E_1 - E_2$ to denote the disparity in unperturbed energy levels, an observation becomes apparent: only setting $\epsilon = 0$, the levels of $\hat{H}$ coincide in energy ($E_+ = E_-$), in particular only when $\Delta E = 0$. This signifies that, devoid of perturbation, a crossing of energy levels is feasible. However, the presence of the generic perturbation forestalls such crossings, even in the case $\Delta E = 0$, engendering the phenomenon of level repulsion.

Now if we calculate the statistics of the level separation $P(E_+ - E_- = \omega) \equiv P(\omega)$, using Eq. (1.14):

$$P(\omega) = N \int dE_1 \int dE_2 \int dH_{12}\, \delta\left(\sqrt{\frac{(E_1 - E_2)^2}{4} + |H_{12}|^2} - \omega\right) \times \\ \times\, p(E_1, E_2, H_{12}) \tag{1.15}$$

where $p(E_1, E_2, H_{12})$ is the probability to have a certain E_1, E_2 and H_{12}.
If we assume this probability Gaussian and we properly normalize the probability distribution $P(\omega)$, one gets the result found by Wigner [21]:

$$P(\omega) = \frac{\pi^2}{2} \omega e^{-\left(\frac{\pi}{4}\right)\omega^2}. \tag{1.16}$$

It turns out that the features described above are not unique to the 2×2 Hamiltonian. This simple example can be generalized to larger matrices using an ensemble of matrices (we will not go into the details), however, even if it does not exist a closed analytic form for this case, it is possible to say that the distribution is qualitatively and quantitatively close to Eq. (1.16) [1].

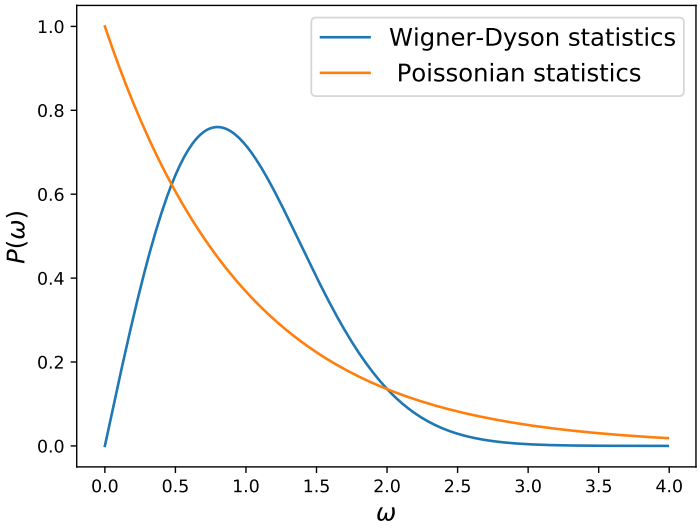

Figure 1.2: Level spacing statistics for different regimes. The Wigner-Dyson formula, Eq. (1.16), is related to the statistics in chaotic systems. The Poissonian distribution, instead, is related to integrable systems.

In conclusion, the manifestation of Wigner-Dyson statistics in the distribution of level spacings illustrated in Fig. 1.2 stands as a characteristic hallmark frequently ascribed to quantum chaotic systems [22]. This phenomenon is in stark contradistinction to the Poissonian statistical regime typifying quantum integrable systems, elucidated in the work by Coux et al. [23]. The discernible prevalence of Wigner-Dyson statistics in such contexts affords discerning insights into the fundamental behaviour of quantum chaotic systems, substantiating their deviation from the ordered regularity inherent to integrable systems.

1.2.1 Matrix elements of operators

The RMT allow us to demonstrate an important statement about the eigenvectors of random matrices:

the eigenstates of a chaotic Hamiltonian in non-fine-tuned bases, are essentially random vectors with no structure.

This statement has consequences in the structure of the matrix elements of Her-

mitian operators. Let a Hermitian operator:

$$\hat{O} = \sum_i O_i |i\rangle\langle i| \quad \text{where} \quad \hat{O}|i\rangle = O_i|i\rangle \tag{1.17}$$

within RMT. For any given random Hamiltonian, for which the eigenkets are denoted by $|m\rangle$ and $|n\rangle$,

$$O_{mn} \equiv \langle m|\hat{O}|n\rangle = \sum_i O_i \langle m|i\rangle\langle i|n\rangle = \sum_i O_i \left(\psi_i^m\right)^* \psi_i^n, \tag{1.18}$$

where $\psi_i^m \equiv \langle i|m\rangle$ and similarly for ψ_i^n. Exploiting the fact that the eigenstates of random matrices in any basis are essentially random orthogonal unit vectors, therefore, to leading order in $\frac{1}{D}$, where D is the dimension of the Hilbert space, we have

$$\overline{\left(\psi_i^m\right)^* \left(\psi_j^n\right)} = \frac{1}{D}\delta_{mn}\delta_{ij}, \tag{1.19}$$

where the average $\overline{\left(\psi_i^m\right)^* \left(\psi_j^n\right)}$ is over random eigenkets $|m\rangle$ and $|n\rangle$. This implies that one has very different expectation values for the diagonal and off-diagonal matrix elements of $\hat{O}$. Indeed, using Eqs. (1.18) and (1.19), we find

$$\overline{O_{mm}} = \frac{1}{D}\sum_i O_i \equiv \overline{O}, \tag{1.20}$$

and

$$O_{mn} = 0, \quad \text{for } m \neq n. \tag{1.21}$$

Now let us consider the quantity:

$$\begin{aligned} \overline{O_{mm}^2} - \overline{O_{mm}}^2 &= \sum_{i,j} O_i O_j \overline{(\psi_i^m)^* \psi_i^m (\psi_j^m)^* \psi_j^m} - \sum_{i,j} O_i O_j \overline{(\psi_i^m)^* \psi_i^m}\ \overline{(\psi_j^m)^* \psi_j^m} \\ &= \sum_i O_i^2 \left(\overline{|\psi_i^m|^4} - (\overline{|\psi_i^m|^2})^2\right) = \frac{3-\beta}{D^2}\sum_i O_i^2 \equiv \frac{3-\beta}{D^2}\overline{O^2} \end{aligned} \tag{1.22}$$

where $\beta = 1$ for ψ_i^m real and $H_{ij} = H_{ji}$ and $\beta = 2$ for ψ_i^m complex and $H_{ij} = H_{ji}^*$. In the first case, we have used the relation $\overline{(\psi_i^m)^4} = 3[\overline{(\psi_i^m)^2}]^2$, while for the second case the relation used is $\overline{|\psi_i^m|^4} = 2(\overline{|\psi_i^m|^2})^2$.
If instead we consider the off-diagonal element of the operator, one gets:

$$\overline{|O_{mn}|^2} - |\overline{O_{mn}}|^2 = \sum_i O_i^2 \overline{|\psi_i^m|^2 |\psi_i^n|^2} = \frac{1}{D}\overline{O^2}. \tag{1.23}$$

Combining these expressions, we see that, to leading order in $1/D$, the matrix elements of any operator can be written as

$$O_{mn} \approx \overline{O}\delta_{mn} + \sqrt{\frac{\overline{O^2}}{D}} R_{mn}, \tag{1.24}$$

where R_{mn} is a random variable, real or complex, with zero mean and unit variance.
In deriving Eqs. (1.20)-(1.23), we averaged over a fictitious ensemble of random Hamiltonians. However, from Eq. (1.24), it is clear that for large D the fluctuations of operators are small and thus one can use the ansatz (1.24) for a given fixed Hamiltonian [1].

1.3 ETH

In 1929, Von Neumann discussed in very detail how statistical mechanics behaviour could emerge in quantum-mechanical systems evolving under unitary dynamics [24].
He studied the behaviour of the macroscopic observables, instead of the wave function or the density matrix of the entire system.
He proved what he named the quantum ergodic theorem, which has been recently discussed in detail by Goldstein et al. [25]. In this last review, the quantum ergodic theorem states:

Let a typical finite family of commuting macroscopic observables. Lifting evolves an initial wave function taken from a microcanonical energy shell, for most times in the long run, the joint probability distribution of these observables, obtained from the unitarily time-evolved wave function, is close to their microcanonical distribution.

This theorem was one of the first studies regarding thermalization in quantum systems. However, comparing the concepts up to now discussed, some problems could arise reading the theorem. For example, the theorem makes no distinction between integrable and nonintegrable systems.
After Von Neumann's work, problems regarding the thermalization of quantum systems are now one of the biggest topics of interest to the scientific community.

Suppose that one prepares an isolated system in a nonstationary state with well-defined mean energy and sub-extensive energy fluctuations.
An observable, particularly its expectation value, is said to thermalize if, during the time evolution of the system, it relaxes to the microcanonical prediction. Whether

the isolated system is in a pure or mixed state is immaterial to the question of thermalization.

To understand the essential ingredients needed for thermalization to occur, let us consider a simple setup in which an isolated system is initially prepared in a pure state $|\psi_I\rangle$ and evolves under a time-independent Hamiltonian $\hat{H}$. We assume that the Hamiltonian has eigenvectors $|m\rangle$ and eigenvalues E_m, that is, $\hat{H}|m\rangle = E_m|m\rangle$. The time-evolving wave function can be written as

$$|\psi(t)\rangle = \sum_m C_m e^{-iE_m t}|m\rangle \tag{1.25}$$

where $C_m = \langle m|\psi_I\rangle$.

We are interested in $t \geq 0$. In particular, let us look at the time evolution of some observable $\hat{O}$, which in the basis of the eigenstates of the Hamiltonian can be written as:

$$\begin{aligned} O(t) \equiv \langle\psi(t)|\hat{O}|\psi(t)\rangle &= \sum_{m,n} C_m^* C_n e^{i(E_m - E_n)t} O_{mn} = \\ &= \sum_m |C_m|^2 O_{mm} + \sum_{m,n\neq m} C_m^* C_n e^{i(E_m - E_n)t} O_{mn} \end{aligned} \tag{1.26}$$

where $O_{mn} = \langle m|\hat{O}|n\rangle$.
As stated before, we say that the observable $\hat{O}$ thermalizes if:

1. after some relaxation time, the average expectation value of this observable agrees with the microcanonical expectation value;

2. temporal fluctuations of the expectation value about the microcanonical prediction are small at most later times.

This implies that the long-time average accurately describes the expectation value of $\hat{O}$ at almost all times and agrees with the microcanonical prediction.

The initial difficulties in reconciling these requirements with Eq. (1.26) are obvious. In the long-time average, the second sum in Eq. (1.26) averages to zero (provided there are no degeneracies) and we are left with the sum of the diagonal elements of $\hat{O}$ weighted by $|C_m|^2$.
At this point, several thoughts may arise:

- since the probabilities $|C_m|^2$ are conserved in time, how is it possible for $\sum_m |C_m|^2 O_{mm}$ to agree with the microcanonical average?

- In many-body systems, the eigenenergies are exponentially close to each other. Therefore, to ensure that the second sum in Eq. (1.26) averages to zero, one might potentially need to wait an exponentially long time. How can we reconcile this with experimental observations?

One can note that if the Hamiltonian $\hat{H}$ is a random matrix, one finds, using Eq. (1.24), that the observables thermalize in the sense just specified. This is because the first sum in Eq. (1.26) becomes independent of the initial state:

$$\sum_m |C_m|^2 O_{mm} \approx \overline{O} \sum_m |C_m|^2 = \overline{O}, \tag{1.27}$$

that is, it agrees with the microcanonical result.
It also becomes clear that exponentially long times may not be needed for relaxation: the off-diagonal matrix elements of $\hat{O}$ are small (they depend on $1/\sqrt{D}$), so by destroying phase coherence between a finite fraction of the eigenstates with a significant contribution to the expectation value, it is possible to approach the infinite-time prediction with high accuracy in a time much shorter.

In order to describe observables in experiments, however, one needs to go beyond the RMT prediction. This is because, in contrast to random matrices, in real systems:

- thermal expectation values of observables depend on the energy density (temperature) of the system;
- relaxation times are observable-dependent.

Hence, there is information in the diagonal and off-diagonal matrix elements of observables in real systems that cannot be found in RMT.

In 1994, Srednicki, after similar ideas introduced by Deutsch in 1991 [26], provided the generalization of the RMT prediction that is needed to describe observables in physical systems [27–29].
Srednicki's ansatz is known as the ETH. It was first shown to apply to realistic quantum systems, where thermalization was observed for a strikingly small number of particles (5 bosons in 21 lattice sites), by Rigol et al.[30]. We have to notice that the smallness of the system they studied precluded them from observing a qualitatively different behaviour between nonintegrable and integrable systems.
In particular, in more detail, Srednicki's ansatz states:

$$O_{mn} = O(\bar{E})\delta_{mn} + e^{-\frac{S(\bar{E})}{2}} f(\bar{E}, \omega) R_{mn} \tag{1.28}$$

where O is the observable in the basis of the eigenstates of a Hamiltonian, $\bar{E} = (E_m + E_n)/2$, $\omega = E_n - E_m$, $A(\bar{E})$ and $f(\bar{E}, \omega)$ are smooth functions, $S(E)$ is the thermodynamic entropy and R_{mn} is a random real or complex variable with zero mean and unit variance ($\overline{R_{mn}^2} = 1$ or $\overline{|R_{mn}|^2} = 1$ respectively)[1].
One has to note also that the matrix elements of observables can be real or complex. It depends on the symmetries of the Hamiltonian and the basis used to

diagonalize it. If the system obeys time-reversal symmetry, the eigenstates of the Hamiltonian can be chosen to be real, and so will be the matrix elements of observables (Hermitian operators). This is not possible if the symmetry is not valid. By taking the Hermitian conjugate of Eq. (1.28), we see that the function $f_O(\bar{E},\omega)$ and the random numbers R_{mn} must satisfy the following relations (the first line for the real case and the second line for the complex case):

$$\begin{aligned} R_{nm} &= R_{mn}, \quad f_O(\bar{E},-\omega) = f_O(\bar{E},\omega) \\ R^*_{nm} &= R_{mn}, \quad f^*_O(\bar{E},-\omega) = f_O(\bar{E},\omega). \end{aligned} \tag{1.29}$$

Moreover, the ETH ansatz reduces to the RMT prediction if one focuses on a very narrow energy window where the function $f_O(\bar{E},\omega)$ is constant.

Let us now describe what the ETH ansatz entails in the thermalization of quantum systems.

1.3.1 ETH and thermalization

Let us focus on the long-time average of observables. If there are no degeneracies in the energy spectrum, which is a reasonable assumption for generic quantum systems after removing all trivial symmetries, we can calculate, using Eq. (1.26):

$$\overline{O} \equiv \lim_{t_0\to\infty} \frac{1}{t_0}\int_0^{t_0} \hat{O}(t)\,dt = \sum_m |C_m|^2 O_{mm} = \mathrm{Tr}\left(\hat{\rho}_{\mathrm{DE}}\,\hat{O}\right) \tag{1.30}$$

where $\hat{\rho}_{\mathrm{DE}}$ is defined in the Eq. (1.12).
Let us also consider the microcanonical average value of the operator $\hat{O}$: $O_{\mathrm{ME}} = \mathrm{Tr}\left(\hat{\rho}_{\mathrm{ME}}\,\hat{O}\right)$, where $\hat{\rho}_{\mathrm{ME}}$ is the density matrix of the microcanonical ensemble (we can use also that of the canonical ensemble, since the equivalence of the ensembles). Then, expanding around the mean energy value $\langle E\rangle$ the value O_{mm}, defined in the Eq. (1.28), we get:

$$O_{mm} \approx O(\langle E\rangle) + (E_m - \langle E\rangle)\frac{dO}{dE}\bigg|_{\langle E\rangle} + \frac{1}{2}(E_m - \langle E\rangle)^2\frac{d^2O}{dE^2}\bigg|_{\langle E\rangle}, \tag{1.31}$$

that applied in Eq. (1.30), we obtain:

$$\overline{O} \approx O(\langle E\rangle) + \frac{1}{2}(\delta E)^2 O''(\langle E\rangle) \approx O_{\mathrm{ME}} + \frac{1}{2}\left((\delta E)^2 - (\delta E_{\mathrm{ME}})^2\right) O''(\langle E\rangle) \tag{1.32}$$

where we have defined $E_m = \langle E\rangle + \delta E$ and used δE_{ME} as the energy fluctuations of the microcanonical ensemble.

In the end, using the ETH ansatz and the fact that the energy fluctuation involved in the above calculations is sub-extensive, we arrive at:

$$\overline{O} \approx O(\langle E \rangle) \approx O_{\mathrm{ME}} \tag{1.33}$$

This result can be seen as the bridge between the classical and the quantum behaviour of operators in many-body systems.

1.3.2 ETH and ergodicity

Having formalized the ETH and observed its implications for the dynamics of isolated quantum systems, we now revisit von Neumann's ergodic theorem and elucidate its connection to ETH.
As previously mentioned, von Neumann's inquiry revolved around comprehending the evolution of observables as the unitary time evolution acts upon the entire set of states originating from the microcanonical ensemble. We will follow the discussion in Ref. [1, 25].

Von Neumann's considerations involve a Hamiltonian operator $\hat{H}$ with eigenstates $|m\rangle$ and corresponding eigenvalues E_m, i.e. $\hat{H}|m\rangle = E_m|m\rangle$. He focused his attention on a microcanonical energy window characterized by a width δE around an energy E. This energy window demarcates a Hilbert space $\mathcal{H}$ of dimension D, spanned by D energy eigenstates $|m\rangle$ with energies $E_m \in (E - \delta E/2, E + \delta E/2)$. Notably, any state within this microcanonical energy range can be expressed as $|\psi\rangle = \sum_{m\in\mathcal{H}} C_m|m\rangle$, where $C_m = \langle m|\psi\rangle$.
Consequently, the Hilbert space $\mathcal{H}$ can be partitioned into orthogonal subspaces $\mathcal{H}_\nu$ of dimensions d_ν, such that $\mathcal{H} = \oplus_\nu \mathcal{H}_\nu$ and $D = \sum_\nu d_\nu$. Finally, observables within $\mathcal{H}$ can be written as $\hat{O} = \sum_\nu \hat{O}_\nu \hat{P}_\nu$, where $\hat{P}_\nu$ is the projector onto $\mathcal{H}_\nu$. It is assumed that both D and d_ν are large.

Defining the expectation value of the observable at time t as

$$O(t) = \langle \psi | e^{i\hat{H}t} \hat{O} e^{-i\hat{H}t} | \psi \rangle \tag{1.34}$$

and its microcanonical average as

$$\langle \hat{O} \rangle_{\mathrm{ME}} = \sum_{m\in\mathcal{H}} \langle m|\hat{O}|m\rangle / D, \tag{1.35}$$

von Neumann's quantum ergodic theorem asserts that if the following conditions are fulfilled:

1. $E_m - E_n \neq E'_m - E'_n$ unless $m = m'$ and $n = n'$, or $m = n$ and $m_0 = n_0$;

2. for any ν, the quantities

$$\max_m \left(\langle m|\hat{P}_\nu|m\rangle - \frac{d_\nu}{D} \right)^2 + \max_{m\neq n} |\langle m|\hat{P}_\nu|n\rangle|^2 \tag{1.36}$$

are exponentially small;

then, for all times t except for a small initial fraction δ of times, it holds that

$$|O(t) - \langle \hat{O} \rangle_{ME}|^2 < \epsilon \langle \hat{O}^2 \rangle_{\mathrm{ME}}, \tag{1.37}$$

where ϵ is a small parameter.

It is possible to see that Eq. (1.36) guarantees that the eigenstate expectation value of $\hat{O}$ is identical to the microcanonical prediction [31]. In fact, we observe that:

$$\langle m|\hat{O}|m\rangle = \sum_\nu O_\nu \langle m|\hat{P}_\nu|m\rangle \approx \sum_\nu O_\nu \frac{d_\nu}{D} = \sum_{m\in\mathcal{H},\nu} O_\nu \frac{\langle m|\hat{P}_\nu|m\rangle}{D} = \langle \hat{O} \rangle_{ME}, \tag{1.38}$$

where the second equality holds up to corrections that are exponentially small as stipulated by Eq. (1.36). We also exploit the property that $\sum_{m\in\mathcal{H}} \langle m|\hat{P}_\nu|m\rangle = d_\nu$. Additionally, we find that:

$$\langle m|\hat{O}|n\rangle = \sum_\nu O_\nu \langle m|\hat{P}_\nu|n\rangle, \tag{1.39}$$

which is exponentially small if $\langle m|\hat{P}_\nu|n\rangle$ satisfies the exponential smallness requirement stated in Eq. (1.36), and if O_ν does not scale exponentially with system size.

Hence, we discern that Eqs. (1.38) and (1.39) precisely mirror the predictions of RMT, i.e. Eq. (1.24), or equivalently, of the ETH within the energy window $\delta E \sim \hbar D/L^2$, where the function $f(\bar{E}, \omega)$ is approximated as a constant.
In conclusion, the ETH is a sufficient condition to have quantum ergodicity [1, 25].

1.3.3 Example of application of ETH

In this section, our objective is to introduce an example that enables us to quantify the concepts delineated in Sec 1.3. Specifically, our focus shall be directed toward scrutinizing the diagonal constituent of the ETH. To this effect, we hereby introduce the spin-1 XYZ Hamiltonian in 1D, defined as:

$$\hat{H} = J \sum_i \left(\hat{S}_i^x \hat{S}_{i+1}^x + \hat{S}_i^y \hat{S}_{i+1}^y \right) + h \sum_i \hat{S}_i^z + J_z \sum_i \hat{S}_i^z \hat{S}_{i+1}^z, \tag{1.40}$$

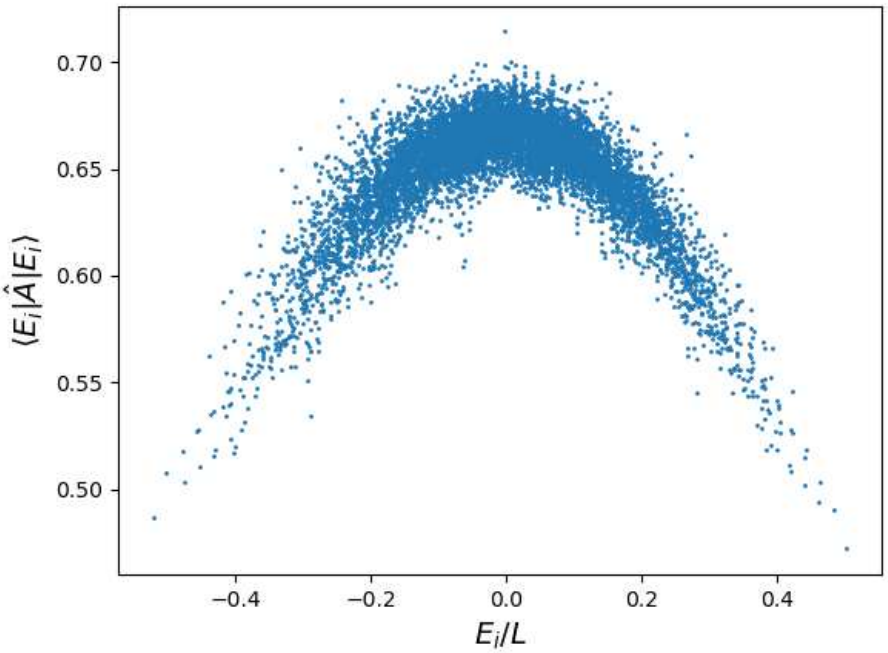

Figure 1.3: We consider $\{J, h, J_z, L\} = \{0.5, 1, 0.5, 10\}$. The plot depicts the expectation values of the eigenstates of the Hamiltonian for $\hat{A} = \frac{1}{L}\sum_i (\hat{S}_i^z)^2$ on the ordinate and the corresponding energy E_i on the abscissa. It is possible to see that all the points align along a smooth curve $A(E_i)$.

where the index $i = 1, \ldots, L$ denotes the lattice sites. The operators $\hat{S}_i^\alpha$ with $\alpha = x, y, z$ are spin-1 operators, while we establish a local basis $|\pm_i\rangle$, $|0_i\rangle$ which are eigenvectors of eigenvalue ± 1 and 0 under $\hat{S}_i^z$ correspondingly. Crucially, this model, by its non-integrable nature, is anticipated to adhere to the ETH [32].
The ETH posits that when considering the diagonal components of an observable, the corresponding values are delineated by a continuous function contingent uniquely upon the energy E_i inherent to the eigenvector $|E_i\rangle$ of the Hamiltonian under consideration. In particular, from Eq. (1.28) it holds:

$$O_{ii} \approx O(E_i). \tag{1.41}$$

To manifest this distinctive feature, we diagonalize exactly the model through the implementation of a Fortran code. The Hamiltonian is evaluated within the context of the zero magnetization sector basis, where the magnetization operator $\hat{M} = \sum_i \hat{S}_i^z$ assumes values of 0 when applied to a basis vector. Concomitantly,

the operator of interest is defined as $\hat{A} \equiv \frac{1}{L}\sum_i \left(\hat{S}_i^z\right)^2$.
In Figure 1.3, a visual representation is provided. Data points demonstrate alignment along a continuous curve $A(E_i)$ as expected from ETH predictions. This behaviour signifies that the eigenstates of the Hamiltonian tend towards conforming to the predictions set forth by the microcanonical ensemble.

Chapter 2

Quantum many-body scar states

Quantum many-body scar states, particular eigenstates of the Hamiltonian, hold now noteworthy importance for multiple reasons, rendering them a subject of pronounced significance within the domain of quantum physics. In this chapter, we will explore the reasons why scar states are crucial and the potential implications they have on our understanding of quantum systems. Here are some key points to consider:

1. *Weak ETH violation and thermalization*: quantum many-body scars violate explicitly the ETH, which is, as said above, a fundamental principle governing the thermalization of closed quantum systems. Scar states resist thermalization and exhibit persistent non-thermal properties, leading to deviations from standard statistical mechanics predictions. Understanding the origin and characteristics of scar states could clarify the boundaries and limitations of ETH, helping us refine our understanding of quantum thermalization. In general, it is important to note that a system that presents scar states violate ETH only in some state, we refer to it as an example of weak ETH violation [33].

2. *Non-equilibrium phenomena*: scar states are fascinating examples of non-equilibrium phenomena in quantum systems. Their long-lived oscillations indicate that these states have unique dynamical properties, unlike most eigenstates that relax to equilibrium. Investigating the mechanisms that sustain these non-equilibrium features could provide valuable insights into the dynamics of complex quantum systems [34, 35].

3. *Quantum information and entanglement*: the study of scar states is relevant to the field of quantum information theory. These states often possess unique entanglement properties and correlations, which could be exploited

for quantum information processing tasks. Moreover, the existence of long-lived coherent oscillations in scar states can be used for quantum memory and control applications [36, 37].

4. *Experimental observability*: advances in experimental techniques have made it possible to probe quantum many-body systems with high precision. Scar states, with their distinctive non-thermal signatures, offer an excellent opportunity to test and validate theoretical predictions in real-world experiments. Observing scar states experimentally could help establish a deeper connection between theory and observation, bridging the gap between quantum theory and practical applications [38, 39].

In conclusion, the significance of quantum many-body scar states extends our comprehension of quantum systems beyond the confines of the ETH. These states provide a distinct perspective into the realm of non-equilibrium dynamics and quantum information within intricate quantum systems. Furthermore, their feasibility for experimental observation positions them as an important tool for validating theoretical conjectures regarding quantum system behaviours. By delving into the intricacies of scar states, we can enrich our understanding of quantum mechanics and potentially uncover novel advancements in the realms of condensed matter physics and quantum information science.

2.1 Ergodicity breaking phenomena

We begin by reviewing aspects of the dynamics of isolated quantum systems. For the sake of concreteness, we focus on a system with L spin-particles and Hamiltonian $\hat{H}$. We are typically interested in the dynamics of a simple wavefunction $|\psi(0)\rangle$ under the Hamiltonian $\hat{H}$, where simple wavefunctions are those that are experimentally accessible, for example, product states or ground states of simple local Hamiltonians. The system evolves the state unitarily, and the wavefunction of the full system at time t is given by $|\psi(t)\rangle = e^{-i\hat{H}t}|\psi(0)\rangle$.

An isolated quantum system without any other symmetries is said to be ergodic or thermal if the reduced density matrix of any small subsystem A of $L_A \ll L$ spins, defined as $\hat{\rho}_A(t) \equiv Tr_B(|\psi(t)\rangle\langle\psi(t)|)$, evolves to a Gibbs density matrix:

$$\lim_{t\to\infty} \hat{\rho}_A(t) = \mathrm{Tr}_B(\hat{\rho}^{eq}) \approx \hat{\rho}_A^{eq} \tag{2.1}$$

where $\hat{\rho}^{eq} = \frac{1}{Z}e^{-\beta\hat{H}}$, B is the complementary subsystem of A, Z is the partition function for the subsystem, and β is an inverse-temperature associated with the

initial state [40].

Most local interacting Hamiltonians are commonly postulated to exhibit a non-integrable nature, thereby complying with complete ergodic behaviour wherein all their eigenstates adhere to the ETH, we refer to it as strong ETH behaviour. Nevertheless, intriguingly, instances of systems manifesting varied levels of ergodicity breakdown have been identified within the quantum realm [40]. We stress that ETH, as discussed in Sec. 1.3.2, serves as a sufficient criterion for ensuring ergodicity in a quantum system.
In this context, two distinctive forms of partial ergodicity deviations have come to light, delineated by the designations Quantum Many-Body Scars (QMBS) and Hilbert Space Fragmentation. These phenomena underscore breaches in ergodicity within isolated quantum systems. Below, we furnish a brief overview of these two phenomena, each contributing to the understanding of ergodicity breakdown within quantum dynamics:

- *QMBS*: some systems exhibit a few highly excited eigenstates that violate diagonal ETH, i.e. they possess atypical features compared to most other eigenstates at the same energy density. These ETH-violating eigenstates in the middle of the spectrum are referred to as QMBS.
  Typically, the number of QMBS grows exponentially slower than the Hilbert space dimension (either polynomially in system size or exponentially with a smaller base), and they constitute an important point to study the thermodynamic limit of the system. Systems in which QMBS appear as equally spaced towers in the spectrum are of particular interest since equal spacings result in perfect revivals from particular initial states, a phenomenon that has been observed in Rydberg atom experiments [7, 41].

- *Hilbert space fragmentation*: another type of ergodicity breaking of a different origin can occur in constrained systems, where the Hilbert space splits into exponentially many dynamically disconnected parts, such that large parts of it are inaccessible to particular initial states.
  Fragmented systems are characterized by eigenstates that can show any scaling of entanglement entropy from area-law to volume-law, depending on the size of the dynamically disconnected part of the Hilbert space they belong to [42].

In the following Sec. 2.2 and Sec. 2.3, we will describe these two scenarios. Additionally, we shall explore potential interrelations that could emerge within this contextual framework.

2.2 QMBS

Much of the present interest surrounding quantum many-body scars finds its inception in an experimental investigation documented within the Ref. [7]. This study discerned unexpected coherent oscillations during the temporal evolution of a system comprising interacting Rydberg atoms. The emergence of these oscillations manifested exclusively when the array was prepared in a specific initial state. In these specific states, the system deviates from the anticipated relaxation behaviour outlined by standard statistical mechanics predictions. For the sake of simplicity and clarity, we stress that in the upcoming Sec. 3, we will abstain from discussing the Rydberg atoms experiment.
This peculiar behaviour prompted a focused inquiry, prompting physicists to scrutinize the underlying model to understand new insights into the realm of QMBS. Given the noteworthy proliferation of models thus far discovered that exhibit QMBS characteristics, a concerted endeavour has arisen to consolidate them into systematic formalisms [43–48]. These endeavours seek to establish unifying frameworks that comprehensively elucidate these phenomena.

The extent of exhaustiveness in these endeavours remains uncertain, and the intricate interconnections among these formalisms remain subjects yet to be rigorously elucidated. Nonetheless, we proceed to provide a comprehensive survey of distinct methodologies aimed at unifying QMBS. These approaches, broadly categorized into two groups that are not mutually exclusive [33], are outlined as follows:

- Shiraishi-Mori embedding formalism,
- spectrum generating algebras-based formalism (SGA-based formalism).

These categories represent diverse paths taken in the pursuit of understanding and unifying QMBS, shedding light on their nature.

2.2.1 Shiraishi-Mori embedding formalism

The inaugural methodological framework for systematically "embedding" precise eigenstates into non-integrable Hamiltonians was pioneered by Shiraishi and Mori (SM), as introduced in Ref. [43]. The crux point of their approach is born from the premise that, within a given model, the ground state can be strategically manipulated by adjusting the model's couplings. This manipulation is executed to transform the ground state into a highly excited state while simultaneously preserving the inherent attributes of its low entanglement characteristics. Through this process, a unique state emerged, distinguished by a discernibly low entanglement entropy positioned within the middle of the energy spectrum. This trait

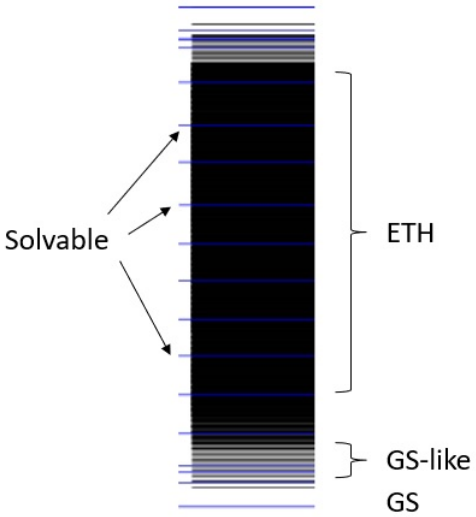

Figure 2.1: Typical example of an energy spectrum with solvable ETH-violating eigenstates that show sub-volume law entanglement in a sea of ETH-satisfying states that show volume-law entanglement. In general, states close to the edges of the spectrum such as the ground state (GS) or low-energy excitations (GS-like) show area-law entanglement and are not expected to satisfy ETH [40].

aligns with the hallmark of systems in which a violation of the ETH occurs [40]. This phenomenon is illustrated in Fig. 2.1.

The SM formalism uses a set of local (generically multi-site) projectors $\{\hat{P}_i\}$ that need not commute with each other, and a target space $\mathcal{T}$ defined as the common subspace of states annihilated by all the projectors, i.e., $\mathcal{T} = \{|\psi_i\rangle : \hat{P}_i|\psi_i\rangle = 0 \ \forall i\}$. Given a target space $\mathcal{T}$, any term $\hat{H}_0$ that commutes with all of the $\hat{P}_i$'s leaves the target space invariant (i.e., $\hat{H}_0|\psi_i\rangle \in \mathcal{T}$ if $|\psi_i\rangle \in \mathcal{T}$ since $\hat{P}_i\hat{H}_0|\psi_i\rangle = \hat{H}_0\hat{P}_i|\psi_i\rangle = 0$). Hence, $\hat{H}_0$ can be diagonalized within $\mathcal{T}$, and the corresponding eigenstates are the eigenstates of any Hamiltonian $\hat{H}_{\rm SM}$ of the form:

$$\hat{H}_{\rm SM} = \sum_i \hat{P}_i\hat{h}_i\hat{P}_i + \hat{H}_0, \quad [\hat{H}_0, \hat{P}_i] = 0 \ \forall i. \tag{2.2}$$

where $\hat{h}_i$ is an arbitrary local operator. The Hamiltonian is constructed to be block-diagonal since $\hat{H}_0$ does not mix states in $\mathcal{T}$ with those in its complement $\overline{\mathcal{T}}$. Thus, $\hat{H}_{SM}$ can be diagonalized in $\mathcal{T}$ and $\overline{\mathcal{T}}$ independently.
The energy eigenvalues of the eigenstates $|\psi_i\rangle_{\mathcal{T}}$ in $\mathcal{T}$ are set entirely by $\hat{H}_0$ and these could be anywhere within the spectrum of $\hat{H}_{SM}$. The other states at the same energy density in $\mathcal{T}$ are, however, expected to reproduce thermal expectation

values, as $\hat{H}_A \equiv \hat{P}_i \hat{h}_i \hat{P}_i$ (and thus $\hat{H}_{SM}$) should be non-integrable for generic Hermitian $\hat{h}_i$.
An alternative perspective is to think of $\mathcal{T}$ and $\overline{\mathcal{T}}$ as dynamically disconnected subspaces that do not couple to each other under the action of $\hat{H}_{SM}$. In other words, $\hat{H}_{SM}$ can be decomposed as

$$\hat{H}_{\mathrm{SM}} = \hat{H}_{\mathcal{T}}^{\mathrm{scar}} \oplus \hat{H}_{\overline{\mathcal{T}}}^{\mathrm{thermal}}. \tag{2.3}$$

Several examples of embedded towers of states lie within the SM construction. In this class of models, we can put the QMBS towers in the spin-1 XY model [49] (it will be studied in detail in Sec. 3) and η-pairing in the Hubbard model [50], although recasting these Hamiltonians in the form of Eq. (2.2) can be difficult.
For illustrative purposes, we consider the introduction of a simplified model, as proposed in the work by Choi et al. [51].
Motivated by recent experimental observations of coherent many-body revivals in a constrained Rydberg atom chain, they constructed a weak quasi-local deformation of the Rydberg blockade Hamiltonian, which makes the revivals virtually perfect. The analysis of the perturbed system suggests them the existence of an underlying non-integrable Hamiltonian which supports an emergent SU(2)-spin dynamics within a small subspace of the many-body Hilbert space.
In light of these insights, the authors proceeded to construct a toy model that interpolates this intrinsic SU(2) structure. This model, while encapsulating the emergent spin dynamics, also accommodates the intriguing phenomenon of Quantum Many-Body Scars (QMBS).
In particular, they considered a system of N spin-1/2 particles on a ring. The subspace $\mathcal{T}$ of the model is defined as the common null space of N projection operators $\hat{P}_{i,i+1} = \frac{1}{4}(1 - \hat{\vec{\sigma}}_i \cdot \hat{\vec{\sigma}}_{i+1})$ onto neighbouring pairs of singlets, where $\hat{\sigma}_i^{\mu}$ ($\mu \in \{x, y, z\}$) are standard Pauli operators at site i.
Such a subspace is spanned by the $N+1$ states of the largest spin representation $s = N/2$ of the SU(2) algebra. The basis states of $\mathcal{T}$ is enumerated by eigenstates of the $\hat{S}_x = \sum_i \hat{\sigma}_x^i/2$ operator, $|s = N/2, m_x\rangle$ with $m_x \in \{-s, \ldots, s\}$ eigenvalue of $\hat{S}_x$. Now, one considers a Hamiltonian of the form

$$\hat{H}_{\mathrm{toy}} = \frac{\Omega}{2} \sum_i \hat{\sigma}_x^i + \sum_i \hat{V}_{i-1,i+2} \hat{P}_{i,i+1}, \tag{2.4}$$

where $\hat{V}_{ij}$ is a generic two-spin operator acting on spins i and j, e.g. $\hat{V}_{ij} = \sum_{\mu\nu} J_{ij}^{\mu\nu} \hat{\sigma}_i^{\mu} \hat{\sigma}_j^{\nu}$ with arbitrary coefficients $J_{ij}^{\mu\nu}$. $\hat{H}_{\mathrm{toy}}$ does not commute with $\hat{P}_{i,i+1}$ nor $\hat{S}_x$; thus, it does not have any obvious local symmetries. However, it can be easily verified that the states $|s = N/2, m_x\rangle \in \mathcal{T}$ are eigenstates with harmonically spaced energies $E = \Omega m_x$. On the other hand, the states in the Hilbert space that

do not belong to $\mathcal{T}$ are affected by the second term in Eq. (2.4), and hybridize to form ergodic eigenstates [51].
In conclusion, the toy model here constructed is reminiscent of Shiraishi and Mori's work, where a set of local projectors was used to embed certain nonergodic energy eigenstates into the bulk of a many-body spectrum.

2.2.2 SGA-based formalism

The towers of QMBS assume fundamental significance within our discourse, owing to their pivotal role in orchestrating many-body revivals, as observed in the context of the Rydberg atom experiment. In this section, we start by elucidating how to construct a tower of states within a quantum many-body system. Subsequently, we delve into characteristics inherent to the presence of such a tower of states composed of QMBS.
In the interest of clarity and simplicity, we opt to provide explicit elucidation of the towers of exact eigenstates within the renowned Hubbard model, known as the η-pairing model. The model facilitates a comprehensive examination of the core attributes inherent to the Spectrum-Generating Algebra (SGA) formalism.

The Hubbard Hamiltonian is [52, 53]:

$$\hat{H}_{\text{Hub}} = \sum_{\sigma\in\{\uparrow,\downarrow\}} \left[-\sum_{\langle r,r'\rangle} t_{r,r'} (\hat{c}^{\dagger}_{r,\sigma}\hat{c}_{r',\sigma} + h.c.) - \mu \sum_{r} \hat{n}_{r,\sigma} \right] + U \sum_{r} \hat{n}_{r,\uparrow}\hat{n}_{r,\downarrow} \tag{2.5}$$

where r labels the sites of a lattice, $\langle r, r'\rangle$ denotes neighbouring sites, and $h_{r,r'}$ denotes the corresponding hopping strength, which is typically chosen to be site-independent. $\hat{c}^{\dagger}_{r,\sigma}$ and $\hat{c}_{r,\sigma}$ denote the fermion creation and annihilation operators on site r, and the on-site fermion number operator is defined as $\hat{n}_{r,\sigma} \equiv \hat{c}^{\dagger}_{r,\sigma}\hat{c}_{r,\sigma}$.

In particular, this model has two SU(2) symmetries, the conventional one and the dynamical one, respectively related to $\hat{S}$ and $\hat{Q}$ operators here defined:

$$\begin{gathered} \hat{S}^{+} = \sum_{r} \hat{c}^{\dagger}_{r,\uparrow}\hat{c}_{r,\downarrow}, \quad \hat{S}^{-} = (\hat{S}^{+})^{\dagger}, \quad \hat{S}^{z} = \frac{1}{2}\sum_{r}(\hat{n}_{r,\uparrow} - \hat{n}_{r,\downarrow}), \\ \vec{S}^{2} = \frac{1}{2}(\hat{S}^{+}\hat{S}^{-} + \hat{S}^{-}\hat{S}^{+}) + (\hat{S}^{z})^{2} \end{gathered} \tag{2.6}$$

and

$$\begin{gathered} \hat{Q}^{\dagger} = \sum_{r} e^{i\pi\cdot r}\hat{c}^{\dagger}_{r,\uparrow}\hat{c}^{\dagger}_{r,\downarrow}, \quad \hat{Q} = (\hat{Q}^{\dagger})^{\dagger}, \quad \hat{Q}^{z} = \frac{1}{2}\left(\sum_{r,\sigma}\hat{n}_{r,\sigma} - L\right), \\ \vec{Q}^{2} \equiv \frac{1}{2}(\hat{Q}^{\dagger}\hat{Q} + \hat{Q}\hat{Q}^{\dagger}) + (\hat{Q}^{z})^{2}. \end{gathered} \tag{2.7}$$

One can demonstrate [40] that:

$$[\hat{S}^z, \hat{S}^+] = \hat{S}^+, \quad [\hat{S}^z, \hat{S}^-] = -\hat{S}^-, \quad [\hat{Q}^z, \hat{Q}^\dagger] = \hat{Q}^\dagger, \quad [\hat{Q}^z, \hat{Q}] = -\hat{Q} \tag{2.8}$$

and

$$[\hat{H}_{\text{Hub}}, \hat{Q}^z] = 0, \quad [\hat{H}_{\text{Hub}}, \hat{\vec{Q}}^2] = 0, \quad [\hat{H}_{\text{Hub}}, \hat{S}^z] = 0, \quad [\hat{H}_{\text{Hub}}, \hat{\vec{S}}^2] = 0. \tag{2.9}$$

Therefore, one can name the states of the system with the quantum numbers given by these two SU(2) symmetry since they satisfy respectively the $\mathfrak{su}(2)$ algebra. However, the main difference between the two symmetries is in the following commutation relations [54]:

$$[\hat{H}_{\text{Hub}}, \hat{S}^+] = 0, \quad [\hat{H}_{\text{Hub}}, \hat{Q}^\dagger] = (U - 2\mu)\hat{Q}^\dagger \equiv \omega \hat{Q}^\dagger \tag{2.10}$$

The commutation relations presented in Eq. (2.10) assume a fundamental role in establishing the framework necessary for the instantiation of a tower of states within the system. In a broader context, we can initiate our discussion by introducing a creation operator $\hat{Q}^+$. Subsequently, we impose the condition that the commutator of $\hat{Q}^+$ with the Hamiltonian H_{SGA} adheres to the following constraint:

$$[\hat{H}_{SGA}, \hat{Q}^+] = \omega \hat{Q}^+, \quad \text{for } \omega \neq 0. \tag{2.11}$$

If $|\psi_0\rangle$ is an eigenstate of $\hat{H}_{SGA}$ with eigenvalue E_0, then $(\hat{Q}^+)^n|\psi_0\rangle$ is also an eigenstate with eigenvalue $E_0 + n\omega$ for any integer $n > 0$ (as long as $(\hat{Q}^+)^n|\psi_0\rangle \neq 0$).

Furthermore, in the study presented in Ref. [55], the researchers derived an exact closed-form expression for the entanglement spectrum of precise many-body excited eigenstates within the framework of the Hubbard model. Interestingly, despite their status as exact excited eigenstates characterized by a higher finite energy density than the ground state energy, these states exhibit a sub-extensive entanglement entropy ($\sim \ln N$) as opposed to the anticipated volume law behaviour ($\sim N$), where N denotes the size of the system.

To really qualify the high excited tower of states as examples of Quantum Many-Body Scars (QMBS), they should be in the middle of the spectrum after resolving symmetries of the system [1, 56].

Refs. [45, 50] showed that local terms can be added to the Hubbard model that breaks either one of the two SU(2) symmetries and translation symmetry while preserving some of the analytically tractable towers as eigenstates. In such models, the remaining towers of states are generically in the middle of the spectrum after resolving all the conventional symmetries of the model and hence are examples of towers of QMBS.

In summary, the SGA formalism hinges upon the utilization of Eq. (2.11) to systematically construct towers of states. When these towers of states, subsequent

to the resolution of all inherent symmetries, exhibit entanglement entropy deviating from the anticipated volume law behaviour within the middle of the spectrum, we are confronted with the manifestation of towers comprising Quantum Many-Body Scars (QMBS) states.

2.3 Hilbert space fragmentation

Hilbert space fragmentation stands as a correlated phenomenon of ergodicity breakdown [40]. Within this section, we engage in an examination of this phenomenon, delving into its parallels and distinctions with QMBS.

Given a quantum system with Hilbert space $\mathcal{H}$ and Hamiltonian $\hat{H}$, we can decompose the Hilbert space into dynamically disconnected subspaces, referred to as Krylov subspaces, as follows:

$$\mathcal{H} = \oplus_{j=1}^{K} \mathcal{K}_j, \quad \mathcal{K}_j = \text{span}_t \left\{ e^{-i\hat{H}t} |\psi_j\rangle \right\} \tag{2.12}$$

where

$$\text{span}_t \left\{ e^{-i\hat{H}t} |\psi_j\rangle \right\} \equiv \text{span} \left\{ |\psi_j\rangle, \hat{H}|\psi_j\rangle, \hat{H}^2|\psi_j\rangle, \dots \right\}, \tag{2.13}$$

denotes the subspace spanned by the time evolution of the state $|\psi_j\rangle$ and K is the number of Krylov subspaces. Note that the $|\psi_j\rangle$'s are chosen such that the subspaces $\mathcal{K}_j$'s are distinct.

Hilbert space fragmentation refers to the phenomenon where the system possesses exponentially many Krylov subspaces, i.e. $K \sim \exp(L)$ for a system of size L. The decomposition outlined in Equation (2.12) presents an elementary task when the states $|\psi_j\rangle$ are eigenstates of the operator $\hat{H}$. This decomposition becomes achievable when the Hamiltonian $\hat{H}$ incorporates specific symmetries that give rise to distinct symmetry quantum numbers associated with different $|\psi_j\rangle$ states within Equation (2.12).

However, for a non-integrable Hamiltonian, the different Krylov subspaces K_j in fragmented systems are not distinguished by quantum numbers corresponding to any obvious local symmetries of $\hat{H}$. Second, for generic systems with conventional symmetries such as Z_2, $U(1)$, or $SU(2)$, the number of Krylov subspaces K either stays constant or grows polynomially with increasing system size, whereas it grows exponentially in fragmented systems [42, 57, 58].

A significant distinction arises from the examination of the relationship between the system's dimension $D_{\max}$ and the dimension of an individual symmetry sector D. In the scenario where the ratio $D_{\max}/D$ for a given sector tends to unity in the thermodynamic limit, it is termed weak fragmentation. Conversely, when this ratio tends to zero for all sectors, the phenomenon is denoted as strong fragmentation.

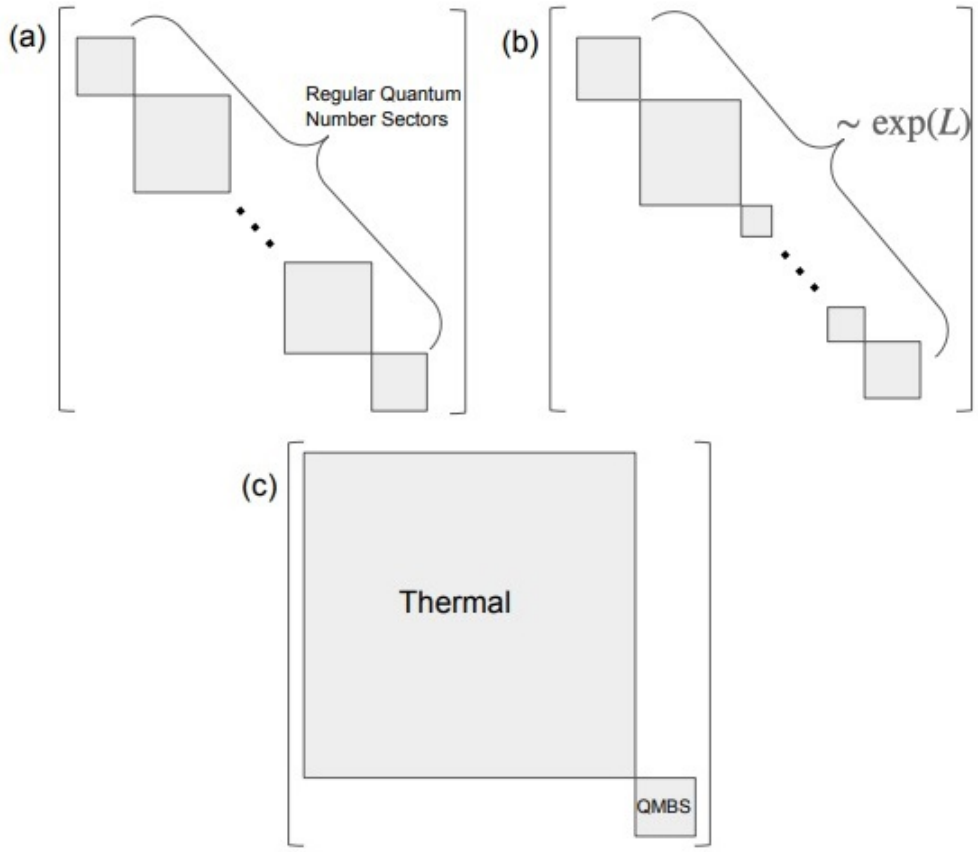

Figure 2.2: Schematic depiction of the block diagonal structure of the Hamiltonian showing the dynamically disconnected Krylov subspaces in systems with (a) conventional symmetries (b) Hilbert space fragmentation (c) QMBS [40].

The phenomenon of fragmented dynamics is acknowledged for its association with scarred characteristics, primarily attributable to its pronounced susceptibility to the initial state. This susceptibility spans a spectrum ranging from localized behaviour to behaviour that converges with thermal expectations, contingent upon the specific dynamical sector from which the system originates. Of particular note, even initial states characterized by low entanglement exhibit distinctive or arrested dynamics, failing to transition to the equilibrium state that aligns with the symmetry quantum numbers of the initial state, thereby encapsulating quintessential features of Quantum Many-Body Scars (QMBS) [33].
In scenarios characterized by strong fragmentation, there emerges an exponential proliferation of dynamically disjoint sectors, as visually depicted in Figure 2.2, resulting in dynamics that resist thermalization, even when initiated from states typifying the system. In contrast, weak fragmentation presents a more pervasive

situation for our discussion, wherein thermalization towards the pertinent thermodynamic ensemble is expected for a broad spectrum of initial states [40].

In conclusion, the phenomena of QMBS and Hilbert space fragmentation have garnered considerable attention, particularly due to their experimental realization in quantum simulators and the availability of an array of exact results and simplified models, a remarkable rarity in the domain of strongly correlated quantum systems. Nevertheless, the array of unresolved challenges we have delineated here is poised to stimulate profound discussions and the exploration of novel physics. However, we stress the fact that the connection will not be an argument in this work.

Chapter 3

Case study for QMBS and asymptotic-QMBS

In this chapter, we explore the spin-1 XY chain model. This model serves as a crucial case study, possessing various violations of the ETH, the presence of QMBS and asymptotic quantum many-body scar states (AQMBS). Our discussion starts with examining the non-integrability of the model, followed by elucidating its principal characteristics. Subsequently, we delve into the phenomena of QMBS and subsequently AQMBS, which stand as our central subjects of inquiry in the future Chapters 4 and 5.

Consider the introduction of the one-dimensional (1D) spin-1 XY model, coupled with an external magnetic field h and an axial anisotropy J_3. The corresponding Hamiltonian can be explicitly stated as follows:

$$\hat{H} = J\sum_j (\hat{S}_j^x \hat{S}_{j+1}^x + \hat{S}_j^y \hat{S}_{j+1}^y) + h\sum_j \hat{S}_j^z + D\sum_j (\hat{S}_j^z)^2 + J_3 \sum_j (\hat{S}_j^x \hat{S}_{j+3}^x + \hat{S}_j^y \hat{S}_{j+3}^y) \tag{3.1}$$

where $j = 1, \ldots, L$ labels lattice sites. The operators $\hat{S}_j^\alpha$ $(\alpha = x, y, z)$ are spin-1 operators, and we choose a local basis $|\pm_j\rangle$, $|0_j\rangle$ whose eigenvalues under $\hat{S}_j^z$ are ± 1 and 0, respectively.
In the context of the system under consideration, the Hamiltonian $\hat{H}$, can be subjected to the condition where J_3 is set to zero. As a consequence, $\hat{H}$ possesses a global U(1) symmetry, which is responsible for inducing rotations of the spins about the z-axis. Depending on the specific boundary conditions at play, the system may further exhibit symmetries related to translation and/or point-group properties. To note that when the dimension of the system is one and Open Boundary Conditions (OBC) are in effect, an additional non-local SU(2) symmetry emerges within $\hat{H}$, as established in Ref. [59]. However, it is worth emphasizing

that the presence of this SU(2) symmetry is not an indispensable requirement for the phenomenon of quantum scarring and can be eliminated by the inclusion of terms incorporating non-zero values of J_3, thereby altering the symmetry landscape of the system [49].

In the subsequent sections of this work, we will adopt OBC as our chosen boundary configuration. With this choice established, we now proceed to engage in a comprehensive examination of the integrability aspects of the model, which is intrinsically intertwined with the symmetrical characteristics inherent to the system.

3.1 Non-integrability of the model

In Chap. 1, we have discussed various methodologies for scrutinizing the concept of system integrability. In this section, our focus will be directed towards a comprehensive examination of level spacing statistics, wherein we introduce the parameters denoted as s, r, and r̃ and their corresponding probability density functions [60]:

1. $$s_i = \frac{E_{i+1} - E_i}{(E_{i+\alpha} - E_{i-\alpha})/\delta E} \tag{3.2}$$
   where $\delta E = 2\alpha$ and E_i are the ordered eigenvalues of the Hamiltonian with $E_0 < E_1 < \ldots < E_N$, E_0 the ground state and E_N the maximum energy;

2. $$r_i = \frac{s_i}{s_{i-1}}; \tag{3.3}$$

3. $$\tilde{r}_i = \frac{\min(s_i, s_{i-1})}{\max(s_i, s_{i-1})} = \min\left(r_i, \frac{1}{r_i}\right). \tag{3.4}$$

The authors in Ref. [60] employed the framework of random matrix theory within the context of Gaussian orthogonal ensembles of matrices (GOE) to derive the analytical expressions for the aforementioned probability distributions. Specifically, the distribution $P(s)$ is identified as the re-scaled Wigner-Dyson distribution, as introduced by the equation (1.16). This yields to the expression

$$P(s) = a \cdot s\, e^{-bs^2}, \tag{3.5}$$

where a and b stand as known normalization constants according to [61]. Meanwhile, the distribution $P(r)$ is governed by the equation

$$P(r) = \frac{1}{Z} \frac{r + r^2}{(1 + r + r^2)^{\frac{5}{2}}}, \tag{3.6}$$

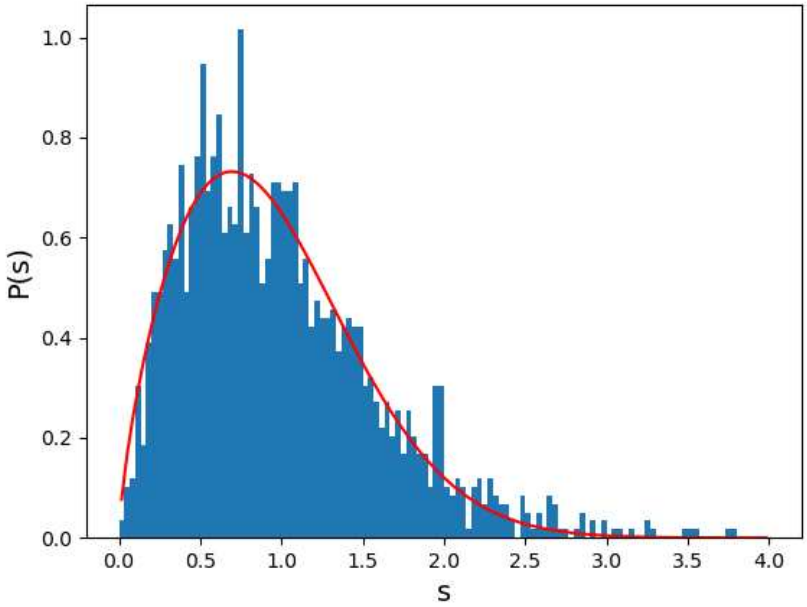

Figure 3.1: P(s) distribution with $\alpha = 10$, $L = 16$, $\hat{M} = \sum_i \hat{S}_i^z = -12$ and $I_\lambda = -1$. The red line is the theoretical Eq. (3.5). The behaviour of the s_i is compatible with the analytical results. [1]

where Z denotes a normalization factor.
The distribution $P(r)$ has the same level of repulsion at small r as $P(s)$, namely $P(r) \sim r$, while for large r the asymptotic behaviour is $P(r) \sim r^{-3}$, contrary to the fast exponential decay of $P(s)$. The Eqs. 3.5 and 3.6 yield an analytic expression for the mean-values $\langle r \rangle$ and $\langle \tilde{r} \rangle$ widely used in the literature as a measure of chaos and integrability.

We have diagonalized the Hamiltonian for small values of L, specifically focusing on a sector of magnetization $\hat{M} = \sum_i \hat{S}_i^z$ where we could gather a significant amount of data for robust statistical analysis. This consideration has taken into account the limitations imposed by the chosen L and the available RAM capacity for the simulations.
Additionally, we have eliminated any inherent symmetries in the model. In this context, our study was confined to the spatial inversion sector characterized by $I_\lambda = -1$, where we are considering the action of the spatial inversion operator $\hat{I}$

[1] If s_i is globally normalized, resulting in its expression as $\frac{E_{i+1}-E_i}{(E_N-E_0)/(N-1)}$, the resultant distribution should exhibit comparability with the depiction in Fig. 1 of the Ref. [49]. Nevertheless, the outcomes we have obtained do not align with the conclusions presented in their work.

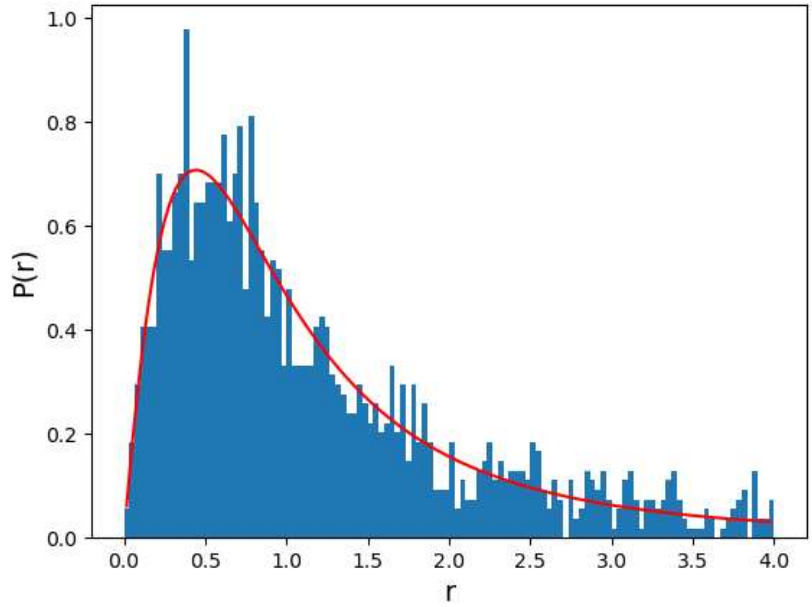

Figure 3.2: $P(r)$ distribution with $\alpha = 10$, $L = 16$, $\hat{M} = \sum_i \hat{S}_i^z$ equal to -12 and $I_\lambda = -1$. The red line is the theoretical Eq. (3.6). The behaviour of the r_i is compatible with the analytical results.

on the wavefunction $\psi(x)$ as $\hat{I}\psi(x) = I_\lambda \psi(-x)$.

The outcomes of our model are depicted in Figures 3.1 and 3.2, with further details presented in Table 3.1. These findings strongly suggest that the Hamiltonian $\hat{H}$ is non-integrable. It is well-known that level statistics alone are not sufficient to guarantee the validity of the ETH. In certain specific cases, a weaker version of the ETH may hold, as suggested by Biroli et al. [62], allowing for a small set of anomalous eigenstates that violate the ETH. Notably, this possibility is remarkable considering that there are no protecting symmetries preventing the anomalous states from mixing with thermal states at the same energy. However, we proceed to demonstrate that this scenario holds for the spin-1 XY model as described in [49].

	Theoretical value	Calculated value
$\langle r \rangle$	1.7781(1)	1.81
$\langle \tilde{r} \rangle$	0.5307(1)	0.53

Table 3.1: Comparison between theoretical [60] and computed $\langle r \rangle$ and $\langle \tilde{r} \rangle$ parameters. $\alpha = 10$, $L = 16$, $M = \sum_i S_i^z = -12$ and $I_\lambda = -1$.

3.2 Quantum many-body scar state of the model

In the previous section, we have demonstrated the non-integrability of the model. Consequently, we expect the model to adhere to the ETH once all symmetries are resolved. However, it is noteworthy that the model has a tower of exact quantum many-body scar states that exhibit a straightforward structure and display distinct properties in comparison to other eigenstates sharing the same energy density.

The system admits a tower of exact bimagnon states:

$$|n,\pi\rangle = \frac{1}{\sqrt{N_{n,\pi}}}(J_\pi^+)^n|\Downarrow\rangle, \tag{3.7}$$

where $n = 0,\ldots,L$, $N_{n,\pi}$ represents a normalization constant, $|\Downarrow\rangle = |-\ldots-\rangle$ is the fully polarized state wherein all spins exist in the eigenstate of $\hat{S}_j^z$ with eigenvalue -1. The bimagnon operator is defined as follows:

$$\hat{J}_k^\pm = \frac{1}{2}\sum_{r=1}^{L} e^{ikr}\left(\hat{S}_r^\pm\right)^2. \tag{3.8}$$

Starting from the family of states $\{|n,\pi\rangle\}_n$, numerous analytical outcomes can be derived [10, 33, 49, 63]:

- The state satisfies a total magnetization equivalent to $M_n = 2n - L$ ($\hat{M} = \sum_i \hat{S}_i^z$) and fulfills the stationary Schrödinger eigenvalue equation:

  $$\hat{H}|n,\pi\rangle = (-Lh + 2nh + LD)|n,\pi\rangle. \tag{3.9}$$

  It's important to note that, for generic values of h and D, the state lies in the middle of the spectrum of the Hamiltonian.

- They form a spin-$L/2$ representation of an SU(2) algebra generated by the raising and lowering operators $\hat{J}_\pi^\pm$:

  $$[\hat{J}_\pi^+, \hat{J}_\pi^-] = 2\hat{J}^z, \quad [\hat{J}^z, \hat{J}_\pi^\pm] = \pm\hat{J}_\pi^\pm, \tag{3.10}$$

  where $\hat{J}^z = \frac{1}{2}\sum_{i=1}^{L}\hat{S}_i^z = \frac{1}{2}\hat{S}^z$.

- The ETH does not hold for these states, given the presence of off-diagonal long-range order in correlation functions, as evidenced by the following expression:

  $$\frac{4}{L^2}\langle n,\pi|\hat{J}_\pi^-\hat{J}_\pi^+|n,\pi\rangle = \left[1 - \left(\frac{2n-L}{2L}\right)^2\right] + \mathcal{O}\left(\frac{1}{L}\right). \tag{3.11}$$

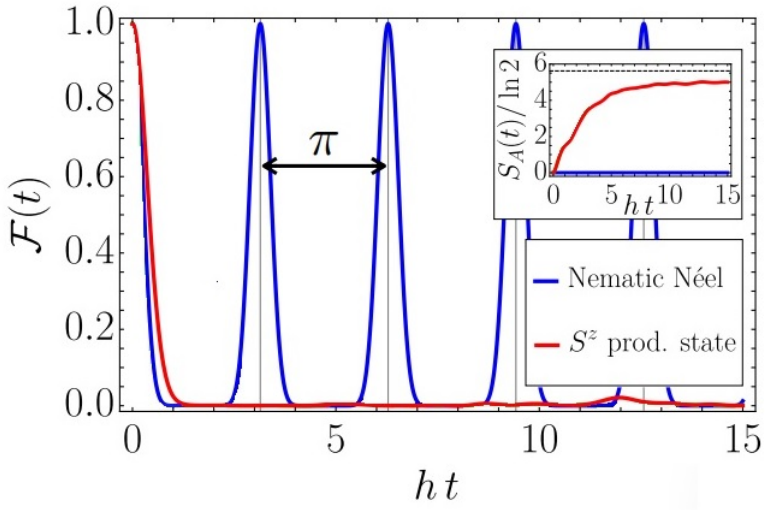

Figure 3.3: Adapted from [33, 49]. $\mathcal{F}(t) = |\langle\psi(0)|\psi(t)\rangle|^2 = |\mathcal{L}(t)|^2$ for various initial states ($L = 8$). The nematic Néel initial state $|\phi\rangle = \otimes_r \left[\frac{|+_r\rangle - (-1)^r|-_r\rangle}{\sqrt{2}}\right]$, state included in Eq. (3.14), exhibits perfect revivals described by Eq. (3.15), while generic initial state decay rapidly (red line). Inset: Entanglement dynamics after a quench, showing that generic initial states lead to rapid entanglement growth and saturation near the value for a random state (dashed line), while the special initial state does not.

It is worth noting that, unless $n = 0$ or L, the right-hand side of the above equation remains finite in the thermodynamic limit. This indicates that the eigenstates $|n, \pi\rangle$ with scarring properties encompass long-range connected correlations (note that $\langle n, \pi|\hat{J}^{\pm}_{\pi}|n, \pi\rangle = 0$).
Conversely, for a generic eigenstate situated in the middle of the energy spectrum, the anticipated value of this correlation function, based on ETH, is derived from the infinite-temperature average:

$$\frac{1}{3^L}\mathrm{Tr}\left(\frac{4}{L^2}\hat{J}^{-}_{\pi}\hat{J}^{+}_{\pi}\right) = \frac{4}{3L}, \tag{3.12}$$

a quantity that diminishes as $L \to \infty$.

- Using simple combinatorics, it is possible to calculate the entanglement entropy of the eigenstates $|n, \pi\rangle$ [49]. For example, the scaling with $\ln(L)$ of the entanglement entropy of the state $|L/2, \pi\rangle$ as $L \to \infty$ can be explicitly

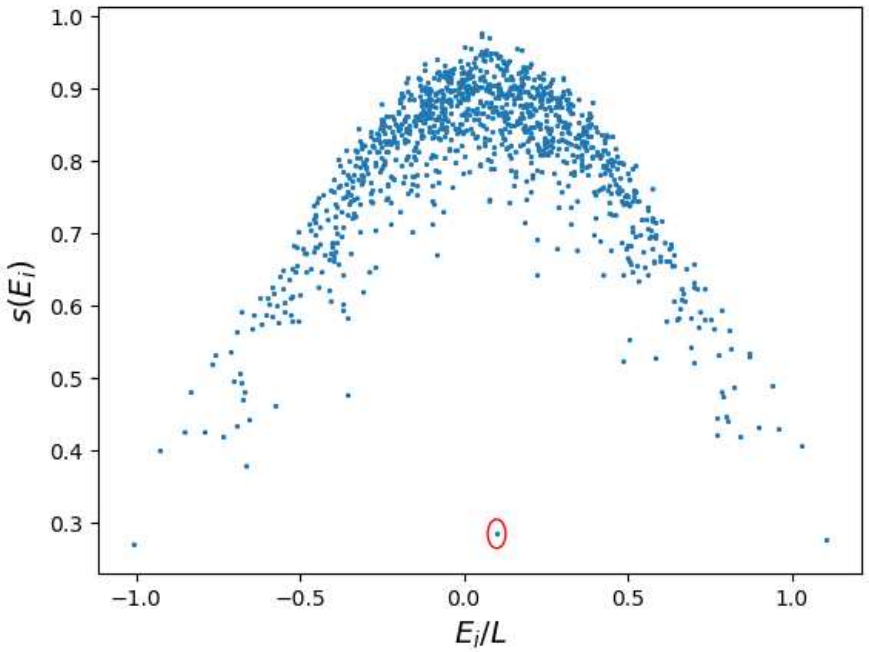

Figure 3.4: We consider the Hamiltonian eigenstates $|E_i\rangle$ in the sector $m = 0$ (we are considering m the eigenvalue of $\hat{M} = \sum_i \hat{S}_i^z$) with parameters $\{J, h, D, J_3, L\} = \{1, 0, 0.1, 0.1, 8\}$. The plot depicts the bipartition entanglement entropy $s(E_i) = -\frac{2}{L}\mathrm{Tr}[\rho_{A,E_i} \log \rho_{A,E_i}]$ where we set A as the set of sites $\{i \,|\, 1 \leq i < L/2\}$ on the ordinate, and the corresponding energy E_i on the abscissa. It is highlighted the scar state point with a red circle. Values computed via exact diagonalization.

shown through saddle point arguments:

$$\lim_{L\to\infty} S_A = \frac{1}{2}\left(\ln\frac{\pi L}{8} + 1\right), \tag{3.13}$$

where $S_A = -\mathrm{Tr}(\hat{\rho}_A \ln \hat{\rho}_A)$, $\hat{\rho}_A = \mathrm{Tr}_B |L/2, \pi\rangle\langle L/2, \pi|$, and Tr_B denotes the trace over sites $1, \ldots, L/2$.
This result contrasts with the prediction of the ETH, as it asserts that finite-energy-density eigenstates of non-integrable models adhere to the volume-law scaling $S_A \sim L$. This different scaling will be visually evident when we analyse the system numerically.

- In the presence of a finite magnetic field h, any state of the form

$$|\psi_0\rangle = \sum_{n=0}^{L} c_n |n, \pi\rangle, \tag{3.14}$$

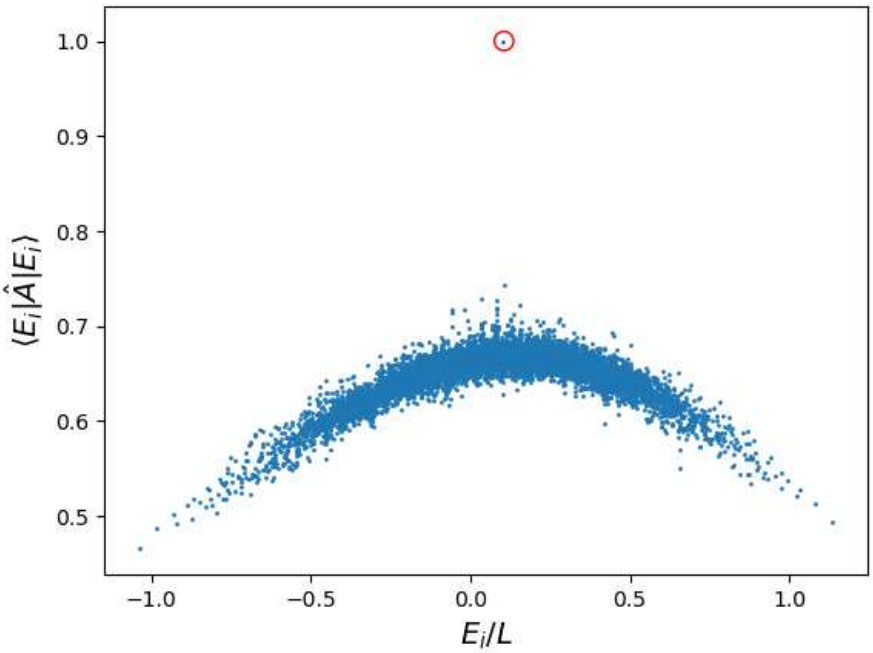

Figure 3.5: We consider $\{m, J, h, D, J_3, L\} = \{0, 1, 0, 0.1, 0.1, 10\}$ (see for the parameters Fig. 3.4). The plot depicts the expectation values of the eigenstates of the Hamiltonian for $\hat{A} = \frac{1}{L}\sum_i (\hat{S}_i^z)^2$ on the ordinate and the corresponding energy E_i on the abscissa. It is highlighted the scar state point with a red circle. Values computed via exact diagonalization.

experiences periodic revivals due to the equally spaced eigenenergies E_n. This phenomenon is more apparent by considering:

$$\mathcal{L}(t) \equiv \langle\psi_0|e^{-i\hat{H}t}|\psi_0\rangle = e^{ihLt}\sum_{n=0}^{L}|c_n|^2 e^{-in(2h)t}, \tag{3.15}$$

Where, up to an unimportant global phase, $\mathcal{L}(t)$ exhibits periodic behaviour with a period of π/h. This time-periodic behaviour stands in contrast to the anticipated behaviour in quantum chaotic systems, where typical initial states are expected to exhibit rapid decay in their expectation values (refer to Fig. 3.3 for numerical simulations).

It is noteworthy to emphasize that the considered model possesses a significant array of analytical results, a circumstance that is relatively uncommon within the domain of quantum many-body interacting systems. The existence of QMBS

states within the model, apart from analytical derivations, can be recognized as outliers with regard to the expectation values of standard operators, for instance, local operators, as observed in numerical simulations.

To offer a numerical exposition of the distinctive attributes displayed QMBS states, we have generated a plot depicting the entanglement entropy, denoted as $s(E_i) = -\frac{2}{L}\mathrm{Tr}[\hat{\rho}_{A,E_i}\log\hat{\rho}_{A,E_i}]$, associated with the reduced density matrix $\hat{\rho}_{A,E_i}$, against the energy E_i of the eigenstates of $\hat{H}$. This density matrix corresponds to the eigenstate $|E_i\rangle$ of the system, wherein our focus is directed towards a specific subsystem A. Specifically, we define A as the set of sites $\{i \,|\, 1 \leq i < L/2\}$ within the chain.
The respective values of both operators are evaluated through exact diagonalization utilizing a Fortran code.
Remarkably, as evidenced by Fig. 3.4 a significant majority of the eigenstates exhibit volume law entanglement entropy behaviour and adhere to the ETH along a smooth curve function of energy. Additionally, these states manifest higher levels of entanglement compared to QMBS states, which solely exhibit an area law, thereby explicitly violating the ETH.
In a broader context, the presence of QMBS states becomes also apparent when considering a more general local operator, for instance, $\hat{A} = \frac{1}{L}\sum_i \left(\hat{S}_i^z\right)^2$, as illustrated in Figure 3.5. Also, in this case, the QMBS state emerges as an outlier, showcasing distinct behaviour in contrast to all other eigenstates.

Up to this point, we have not only demonstrated the presence of QMBS within the model but also characterized their intrinsic properties. Moving forward, we will introduce in the model a family of states that exhibit particular resemblances to the QMBS states discussed in this section.

3.3 Asymptotic quantum many-body scar states

Up to this point, we have brought attention to deviations from the ETH exhibited by QMBS states, which are specific eigenstates of the Hamiltonian.
In a recent investigation detailed in Ref. [10], novel combinations of states, which are generally non-eigenstates of the Hamiltonian, exhibit a semblance of behaviour similar to QMBS in the thermodynamic limit within the framework of the model described by Eq. (3). These states have been termed asymptotic Quantum Many-Body Scar (AQMBS) states.
In this section, we shall introduce and examine the fundamental attributes of these newly discovered states.

AQMBS arise as linear combinations of "thermal" eigenstates that individually

adhere to the expected behaviour stipulated by the ETH. Hence, considering a fixed value of L and allowing t to approach infinity ∞, one could expect that the AQMBS states progressively converge towards statistical predictions. However, the authors of the study [10] have effectively demonstrated that AQMBS possess attributes characterized by constrained entanglement and distinctive signatures of slow relaxation dynamics. Consequently, the presence of AQMBS introduces an alternative avenue to QMBS, for potential deviations from the ETH.
Consider the family of states within the context of Eq. (3.1) as follows:

$$|n,k\rangle = \frac{1}{\sqrt{N_{n,k}}}\hat{J}_k^+ \left(\hat{J}_\pi^+\right)^{n-1} |\Downarrow\rangle, \tag{3.16}$$

where $N_{n,k}$ represents the usual normalization constant, already introduced in Eq. (3.7). Let us now enumerate several properties of $|n,k\rangle$:

- They are deformations of exact QMBS. Studies involving models where such categories of multimagnon states serve as exact eigenstates have been explored in Ref. [64]. The referenced work establishes that these states do not qualify as eigenstates of the spin-1 XY model when $k \neq \pi$.

- For $k \neq \pi$ and k an integer multiple of $\frac{2\pi}{L}$, $\langle n,k|n',\pi\rangle = \delta_{n,n'}\delta_{k,\pi}$ for any $1 \leq n,n' \leq L-1$ [10].

- The expectation energy of these states does not depend on k and reads [10]

$$\langle n,k|\hat{H}|n,k\rangle = -Lh + 2nh + LD. \tag{3.17}$$

- An estimation of the bipartition entanglement entropy can be computed as detailed in references such as [40, 49, 55, 65]. In particular, in Ref. [10], it was demonstrated that by considering a bipartition with $L_A = L_B = L/2$ and focusing on states characterized by an extensive number of bimagnons (those with $n = \alpha L$ and $0 < \alpha < 1$), these states exhibit the following bipartition entanglement entropy relationship: $S_A \sim \log L + \log \alpha$. For the AQMBS states $|n,k\rangle$, an additional correction of at most $\log 2$ is observed. Specifically, $S_A \sim \log 2 + \log \alpha + \log L$.

- The characterization of the states presented in Eq. (3.16) is attainable through the computation of the energy variance ΔH^2 (we report the result of the calculation in OBC):

$$\Delta H^2 = 4\left(J^2\cos^2\left(\frac{k}{2}\right)\left(1-\frac{1}{L}\right) + J_3^2\cos^2\left(\frac{3k}{2}\right)\left(1-\frac{3}{L}\right)\right) \tag{3.18}$$

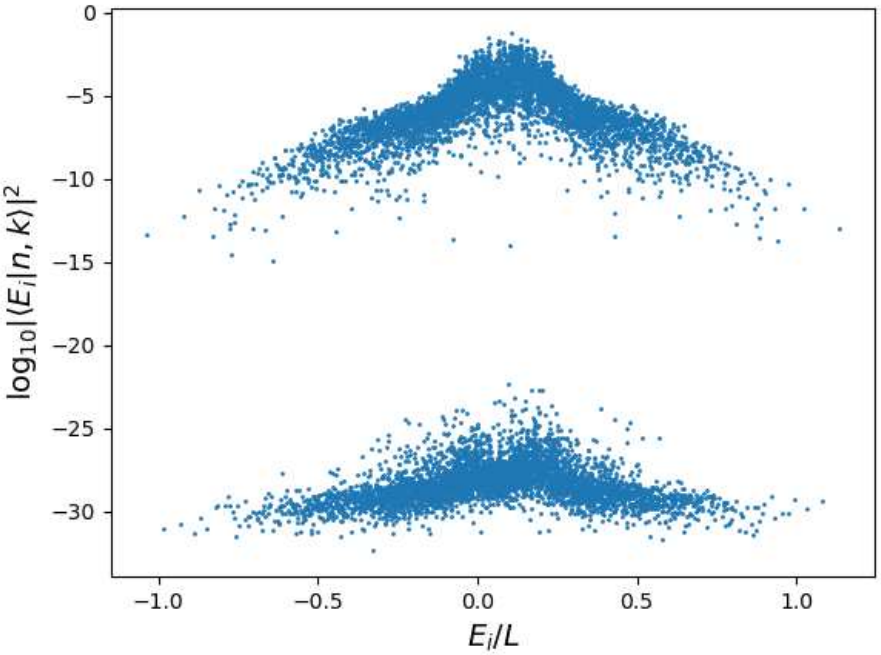

Figure 3.6: Projection of AQMBS $|n,k\rangle$, $n = L/2$, $k = \pi - \frac{2\pi}{L}$, $L = 10$ with eigenstates $|E_i\rangle$ of the Hamiltonian in the sector parameters $\{m, J, h, D, J_3\} = \{0, 1, 0, 0.1, 0.1\}$. Two bands are visible: the bottom one is compatible with the numerical 0; from the top one is possible to see the small variance ΔH^2 of the state $|n,k\rangle$. Values computed via exact diagonalization.

Among the states defined in Eq. (3.16), only the $|n,\pi\rangle$ states qualify as eigenstates of the Hamiltonian, as $\Delta H^2 = 0$ solely for $k = \pi$.
In cases where $k \neq \pi$, the state $|n,k\rangle$ must inevitably be a linear superposition of energy eigenstates of $\hat{H}$. These eigenstates predominantly span a range centred around the same energy as $|n,\pi\rangle$, with a width of approximately ΔH, as depicted in Fig. 3.6.
A notable observation arises when $k \neq \pi$ and k correspond to an integer multiple of $\frac{2\pi}{L}$. In such instances, $|n,\pi\rangle$ is not included in the set of states that compose the AQMBS due to orthogonality constraints, therefore we deduce that states $|n,k\rangle$ must inherently constitute linear superpositions of "thermal" eigenstates.

At this point, it is important to underscore three distinctive attributes that render the AQMBS states particularly interesting:

1. They manifest a limited amount of entanglement, while simultaneously pos-

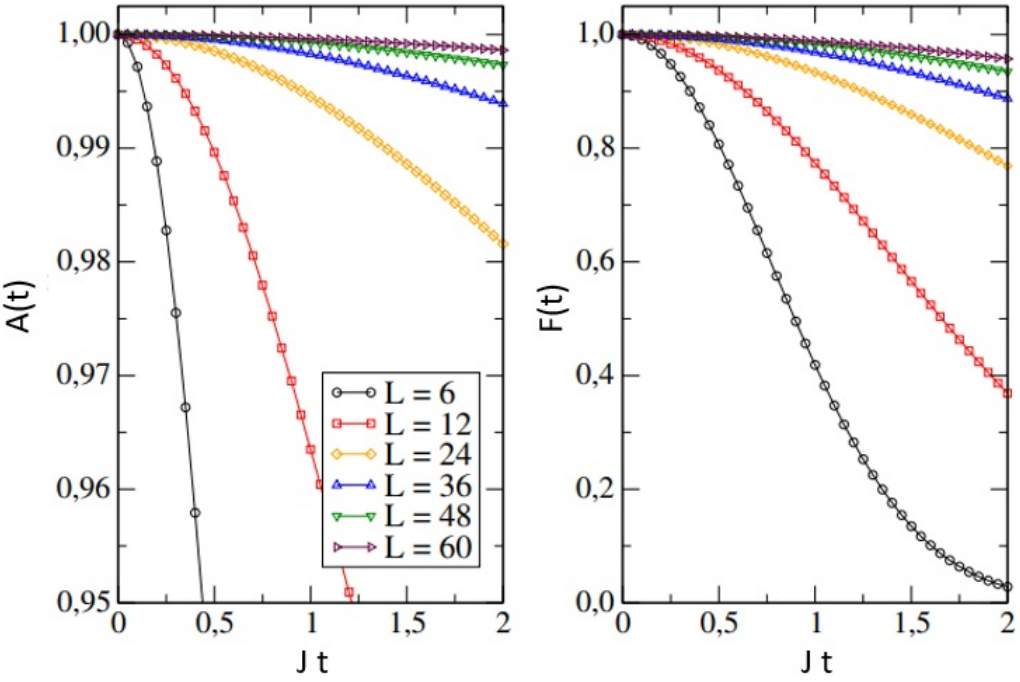

Figure 3.7: Adapted from Ref. [10]. Properties of the state $e^{-i\hat{H}t}|n,k\rangle$ for $n = \frac{L}{2}$ and $k = \pi - \frac{2\pi}{L}$ as a function of time for various system sizes L. Left: time evolution of the operator $\hat{A} = \frac{1}{L}\sum_i \left(\hat{S}_i^z\right)^2$. Right: time evolution of the survival probability with the initial state $F(t) = |\langle n,k|e^{-i\hat{H}t}|n,k\rangle|^2$.

sessing an extensive amount of energy.

2. They display slow dynamics, i.e. in terms of the survival probability $F(t) = |\langle n,k|e^{-i\hat{H}t}|n,k\rangle|^2$, due to the small ΔH^2.

3. As the system approaches the thermodynamic limit ($L \to \infty$), when considering the state $|n,k\rangle$ with $k = \pi + \frac{2\pi}{L}m$ and $m \in \mathbb{Z}$, the scaling behavior of ΔH^2 is proportional to $\frac{1}{L^2}$, resulting in the convergence of ΔH^2 towards zero. This leads to the term asymptotic QMBS (AQMBS), signifying that the system gradually reaches a state of increasing immobility over timescales that demonstrate polynomial growth with the system size (see Fig. 3.7), beyond encompassing the main characteristics associated to QMBS states.

Importantly, the three properties we have described constitute pivotal characteristics that significantly diverge from typical behaviour. Construct states that are

linear combinations of thermal eigenstates, and simultaneously possess a small energy variance (resulting in slow relaxation) while maintaining low entanglement represents a difficult challenge. A typical state with low entanglement often exhibits an energy variance that increases with the system size, implying shorter relaxation times [66] (where $F(t)$ decays on timescales that decrease with system size), while the expectation values of typical observables relax on timescales that do not undergo drastic changes with system size [67–74].

The existence of AQMBS states might lead to the temptation of inferring a form of "non-thermal" behaviour [75] or even a potential violation of the ETH within the "thermal" states orthogonal to the exact QMBS states, even at finite system sizes. However, it is important to stress that the ETH encompasses two fundamental aspects [1, 27, 76], addressing both diagonal and off-diagonal matrix elements of local operators within the energy eigenbasis. The diagonal matrix elements govern the late-time expectation values of observables, and we do not expect a violation of diagonal ETH since the asymptotic QMBS states eventually thermalize. On the contrary, the relaxation timescale is influenced by both the energy variance of the initial state and the off-diagonal matrix elements, though establishing a precise connection remains intricate [67].

In conclusion, the set of characteristics outlined above leads us to consider the possibility of an off-diagonal ETH violation, particularly within a portion of the Hamiltonian spectrum.

Chapter 4

Slow dynamics and function $f(\bar{E}, \omega)$

In this chapter, we delve into the significance of AQMBS states introduced in the previous chapter, particularly in relation to the off-diagonal elements of the ETH. We have already highlighted a crucial aspect of AQMBS: their slow dynamics and the prolonged relaxation time as they approach the equilibrium state. This remarkable behaviour is intimately tied to the off-diagonal properties of the observables under consideration, with the $f(\bar{E}, \omega)$ introduced in Chap. 1. We will investigate the feasibility of establishing a relation between the slow dynamics and the spectral properties of observables.
We will analyze, in this chapter, the relation by examining the system within the magnetization sector, specifically when the magnetization parameter is set to zero (i.e., $m = 0$). This choice is motivated by the objective of obtaining a sufficient quantity of data to conduct a rigorous statistical analysis. Furthermore, we select the quantum state denoted as $|n, k\rangle$, where $k = \pi - \frac{2\pi}{L}$, primarily due to its distinctive ΔH^2 scaling properties, as described in Sec. 3.3.

4.1 AQMBS and thermalization

We start our analysis by delineating critical distinctions between states of AQMBS and the category we designate as a "thermal" state. For illustrative purposes, we adopt the staggered state denoted as $|+-+-\ldots+-\rangle$ as our representative example of a "thermal" state.
The choice of the staggered state is motivated by its equating energy with that of the $|n, k\rangle$ state while exhibiting a divergent energy variance, consequently leading to distinct relaxation dynamics towards the equilibrium state. Specifically, under the conditions introduced in the beginning of this chapter, the following holds:

$$\langle n, k|\hat{H}|n, k\rangle = \langle +-\ldots+-|\hat{H}|+-\ldots+-\rangle = LD. \tag{4.1}$$

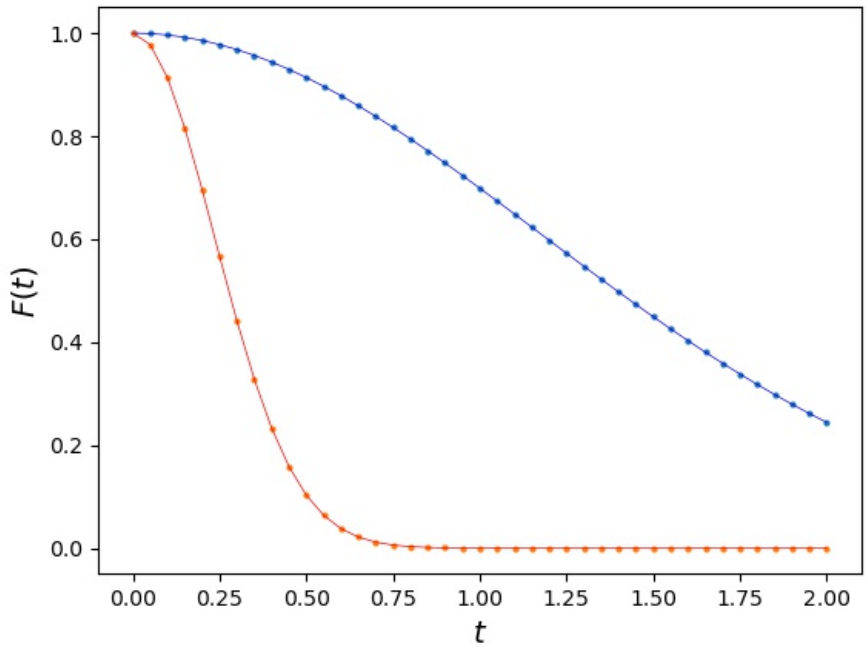

Figure 4.1: Time evolution $e^{-i\hat{H}t}$ of $|n,k\rangle$ state (blue points) and of the staggered state $|+-\ldots+-\rangle$ (orange points). Parameter used for $|n,k\rangle$: $n = L/2$, $k = \pi - \frac{2\pi}{L}$. Hamiltonian parameters sector $\{m, J, h, D, J_3, L\} = \{0, 1, 0, 0.1, 0.1, 10\}$.

In contrast, the variance for the staggered state is expressed as:

$$\langle +-\ldots+-|\Delta H^2|+-\ldots+-\rangle = (J^2 + J_3^2)L. \tag{4.2}$$

Meanwhile, for the AQMBS state, the validity of Equation (3.18) persists.
Remarkably, as the system size approaches infinity (referred to as the thermodynamic limit), the variance ΔH^2 scales proportionally with L in the staggered state, which increases with system size. This stands in contrast to the behaviour observed in the variance of the AQMBS state with $k = \pi - \frac{2\pi}{L}$, where, in the thermodynamic limit, ΔH^2 scales inversely with $\frac{1}{L^2}$, resulting in a decrease as the system size grows.
As discussed in Chap. 3, the variance plays a pivotal role in influencing the relaxation time. From Fig. 4.1, it becomes evident that, despite both states possessing identical energies, the staggered state exhibits a rapid decay and departs significantly from its initial state much more rapidly in comparison to the behaviour observed in the AQMBS state. An additional implication of the disparate variances ΔH^2 is manifest in the projection of the state onto the eigenstates of the

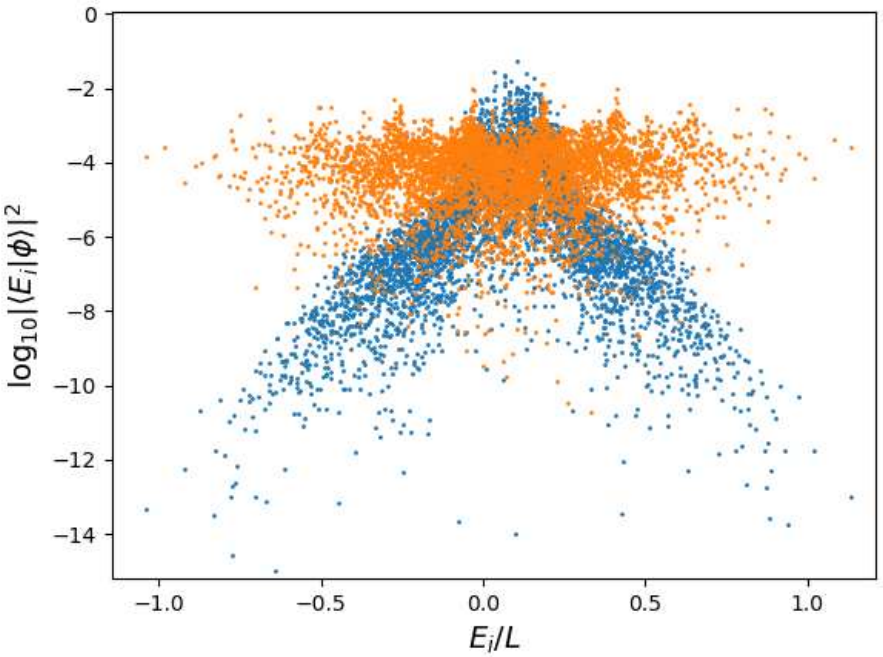

Figure 4.2: Comparison of projection of staggered state $|\phi\rangle = |+-\ldots+-\rangle$ (orange points) and AQMBS $|\phi\rangle = |n,k\rangle$ (blue points), $n = L/2$, $k = \pi - \frac{2\pi}{L}$, $L = 10$ with eigenstates $|E_i\rangle$ of the Hamiltonian in the parameters sector $\{m, J, h, D, J_3\} = \{0, 1, 0, 0.1, 0.1\}$. The discernible disparity in the distribution of data points is a consequence of the variance dissimilarity in energy between the "thermal" state and the AQMBS state.

Hamiltonian. As visible in Figure 4.2, the staggered state, by virtue of its higher variance ΔH^2 with respect to the AQMBS, exhibits a broader spectral overlap with the eigenstates of the Hamiltonian.

In conclusion, the observed variance disparity constitutes a potentially discriminative instrument for distinguishing between a "thermal" state and an AQMBS, thereby affording us the capability to predict the system's behaviour as it evolves towards the equilibrium state.

4.2 Study of off-diagonal matrix elements

In Sec. 4.1, we have previously delineated features associated with slow dynamics, characterized by an extended relaxation time toward the equilibrium state. In the present section, we initiate an examination of the off-diagonal matrix elements of

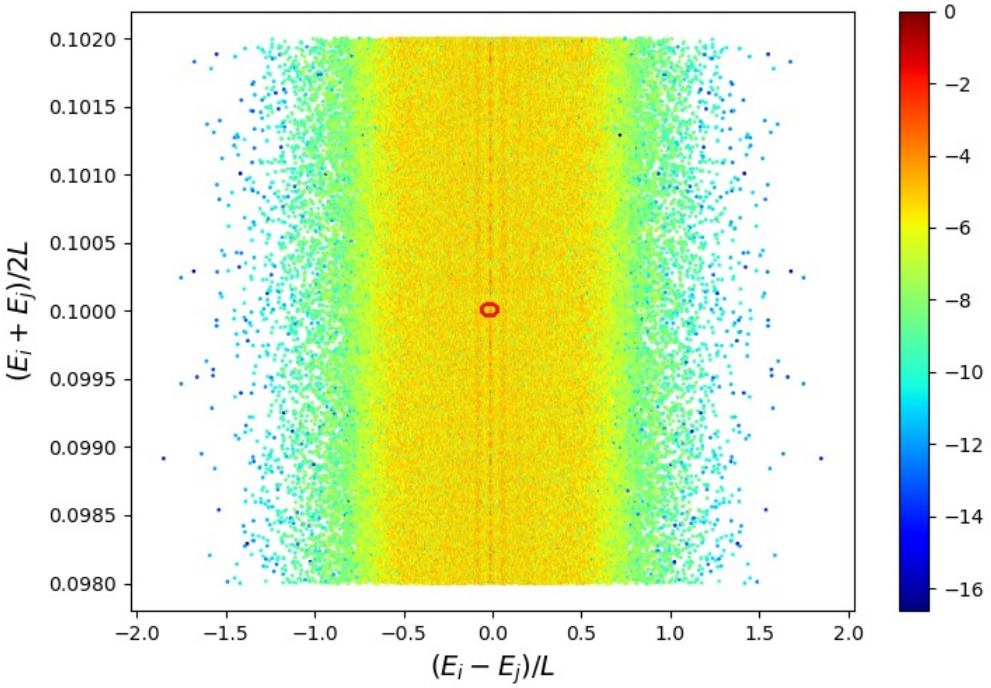

Figure 4.3: Matrix elements $|\langle E_i|\hat{A}|E_j\rangle|^2$ with Hamiltonian parameters $\{m, J, h, D, J_3, L\} = \{0, 1, 0, 0.1, 0.1, 10\}$. It is possible to see in the z-axis the matrix elements in $\log_{10}$-scale with a value greater than 10^{-20}. We consider the elements in the set described by a fixed mean energy around the QMBS (red circle) $\bar{E}_{\text{QMBS}} \equiv [(E_i + E_j)/2L]_{\text{QMBS}} = 0.1$ and $\delta\bar{E}_{QMBS} = 0.002$. This dataset will be used for further analysis in this chapter. Values computed via exact diagonalization.

a local observable.

Specifically, we consider the observable operator $\hat{A}$, defined as $\hat{A} = \frac{1}{L}\sum_i \left(\hat{S}_i^z\right)^2$, within the theoretical framework of the spin-1 XY chain, as introduced in Chapter 3. In Fig. 4.3, our analysis centres on a distinct energy interval, specifically focused around the QMBS energy, which is demarcated by the red circle in the figure. Within this energy range, our study is directed towards a subset of matrix elements associated with the operator $\hat{A}$, expressed as $A_{ij} = \langle E_i|\hat{A}|E_j\rangle$, where E_i and E_j correspond to the energies of the eigenstates of the Hamiltonian $|E_i\rangle$ and $|E_j\rangle$.

These matrix elements, depicted along the z-axis in a logarithmic scale and ex-

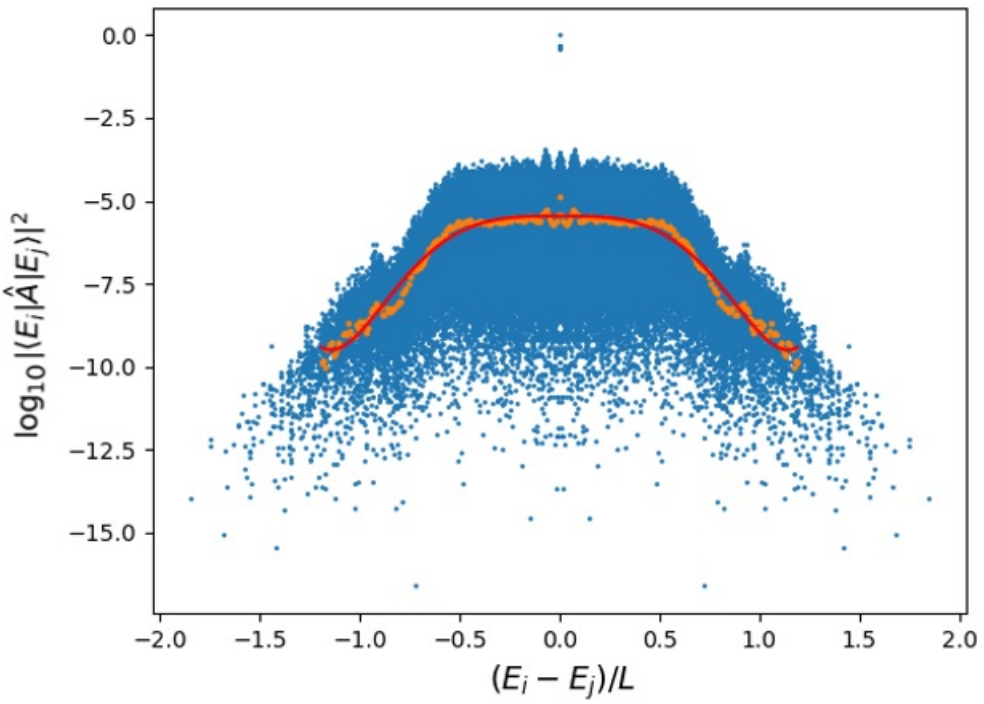

Figure 4.4: Matrix elements $|\langle E_i|\hat{A}|E_j\rangle|^2$ within the energy band $\bar{E}_{\text{QMBS}} = 0.1$ and width $\delta\bar{E}_{\text{QMBS}} = 0.002$ (see Fig. 4.3), with Hamiltonian parameters $\{m, J, h, D, J_3, L\} = \{0, 1, 0, 0.1, 0.1, 10\}$. The "averaged" matrix elements (orange points) are constructed taking intervals of 250 points and then averaging the points both in x and y axis; the red line is a representation of the $|f(\bar{E}, \omega)|^2$, up to a normalization factor. The function plotted on the orange point is $ax^4 + bx^2 + c + d\cos(x)$.

hibiting values greater than the threshold of 10^{-20}, thus belong to the same mean energy interval. To be precise, we set this mean energy, denoted as $\bar{E}_{\text{QMBS}}$, equivalent to D, the parameter met in Eq (3) (to note that $\langle n, \pi|\hat{H}|n, \pi\rangle/L = D$). Additionally, we introduce a variation in this mean energy, denoted as $\delta\bar{E}_{QMBS}$, set at a fixed value of 0.002.

The central focus of our investigation within this analysis is around the examination, at fixed mean energy, of the dependence of the matrix elements on the energy difference parameter, denoted as $\omega = E_i - E_j$.
As depicted in Figure 4.3, it becomes evident that the matrix elements exhibit significantly higher magnitudes in proximity to the diagonal elements ($E_i = E_j$)

when compared to the values observed in the off-diagonal region. This observed behaviour, at least in a qualitative sense, conforms to the ETH hypothesis of Eq. (1.28), particularly with regard to the distinctive decay manifested in the off-diagonal elements.
The examination of plots of this nature will prove instrumental in establishing a correlation between the spectral characteristics of observables and the slow dynamics present in the system.

4.3 Thermalization and $f(\bar{E}, \omega)$

In the previous section, we embarked upon an investigation centred on the off-diagonal matrix elements, specifically focusing on the squared modulus $|A_{ij}|^2$, associated with the local observable $\hat{A}$. Within the framework of the ETH, the off-diagonal elements are described by the function $f(\bar{E}, \omega)$. Our current objective is to establish a connection between the study presented in Fig. 4.3 and a well-defined function $f(\bar{E}, \omega)$.
Let us start with the ETH (see Chap. 1):

$$A_{ij} = A(\bar{E})\delta_{ij} + e^{-\frac{S(\bar{E})}{2}} f(\bar{E}, \omega) R_{ij}. \tag{4.3}$$

Specifically, we focus on matrix elements that fall within the energy interval defined as $\mathcal{E} = [\frac{E_i+E_j}{2} - \delta\bar{E}, \frac{E_i+E_j}{2} + \delta\bar{E}]$, which can be expressed as $\mathcal{E} = [\bar{E} - \delta\bar{E}, \bar{E} + \delta\bar{E}]$ defining $\bar{E} = \frac{E_i+E_j}{2}$, and we introduce the energy difference $\Omega = [(E_i - E_j) + \delta\omega, (E_i - E_j) - \delta\omega] \equiv [\omega - \delta\omega, \omega + \delta\omega]$, where we define $\omega = E_i - E_j$. In our analysis, we shall scrutinize the squared modulus $|A_{ij}|^2$, incorporating typical global scaling factors within the function $f(\bar{E}, \omega)$, as outlined below:

$$\begin{aligned}
\sum_{\substack{E_i,E_j \\ E_i \neq E_j \\ (E_i+E_j)/2 \in \mathcal{E} \\ E_i - E_j \in \Omega}} |A_{ij}|^2 &\overset{(1)}{=} \sum_{\substack{E_i,E_j \\ E_i \neq E_j \\ (E_i+E_j)/2 \in \mathcal{E} \\ E_i - E_j \in \Omega}} |f(\bar{E}, \omega)|^2 |R_{ij}|^2 e^{-S(\bar{E})} = \\
&\overset{(2)}{=} e^{-S(\bar{E})} |f(\bar{E}, \omega)|^2 \sum_{\substack{E_i,E_j \\ E_i \neq E_j \\ (E_i+E_j)/2 \in \mathcal{E} \\ E_i - E_j \in \Omega}} |R_{ij}|^2 = \\
&\overset{(3)}{\simeq} \frac{\alpha\, |f(\bar{E}, \omega)|^2}{\sum_{E_i \in \mathcal{E}} 1}.
\end{aligned} \tag{4.4}$$

In (1), we have invoked Eq. (4.3), in (2), the functions $S(\bar{E})$ and $f(\bar{E}, \omega)$ are explicitly noted to be independent of the individual energies E_i and E_j and in

(3) we exploit the fact that $\overline{|R_{ij}|^2} = 1$, approximating $|R_{ij}|^2$ to 1. We have also introduced the constant

$$\alpha \equiv \sum_{\substack{E_i,E_j \\ E_i \neq E_j \\ (E_i+E_j)/2 \in \mathcal{E} \\ E_i - E_j \in \Omega}} 1 \tag{4.5}$$

as the number of microstates presents into a small interval with fixed $\bar{E}$ and ω and the entropy $S(\bar{E})$ as:

$$S(\bar{E}) = \log \tilde{\Omega}(\bar{E}) \tag{4.6}$$

where

$$\tilde{\Omega}(\bar{E}) = \sum_{E_i \in \mathcal{E}} 1 \tag{4.7}$$

is the number of microstates in an interval with fixed $\bar{E}$.
Therefore, the study of the quantity $|A_{ij}|^2$ in a band of energy, fundamentally involves the assessment of the squared modulus of a well-defined function $f(\bar{E}, \omega)$.
Building upon the preceding calculations, our objective is to investigate the patterns exhibited by the matrix elements within a defined energy range. Specifically, we concentrate our analysis on an energy band situated around the energy associated with the QMBS, as explored in the previous section. Subsequently, we will recover the corresponding function $f(\bar{E}, \omega)$ and use it as a bridge between thermalization of the states and spectral properties.
Starting from Fig. 4.3, our approach involves projecting the data points onto the x-z-plane. Subsequently, we partitioned these points into intervals, with each interval accommodating 250 data points. Within each interval, we performed an averaging operation, resulting in a final dataset comprising "averaged" points. These "averaged" data points serve as the basis for fitting the function $|f|^2$. This systematic procedure ensures a rigorous and precise characterization of the data, enhancing the reliability of our analysis [1]. Fig. 4.4 illustrates the method previously delineated. Notably, the function $|f|^2$ exhibits a discernible plateau in proximity to the diagonal matrix elements and subsequently diminishes as it extends toward the edges of the distribution.

Moving forward, we focus again to Fig. 4.4, but with a particular condition imposed. Here, we confine our consideration to the distribution of matrix elements calculated exclusively using eigenstates of the Hamiltonian that simultaneously exhibit overlaps with either $|n, k\rangle$ or $|+-+-\ldots+-\rangle$ greater than a user-defined threshold. As elucidated in Sec. 4.1, we stress that the magnitude of these overlaps is inherently contingent upon the energy variance ΔH^2 of the state.
Upon examining the new distributions of $|A_{ij}|^2$ in Fig. 4.5, we observe two significant trends:

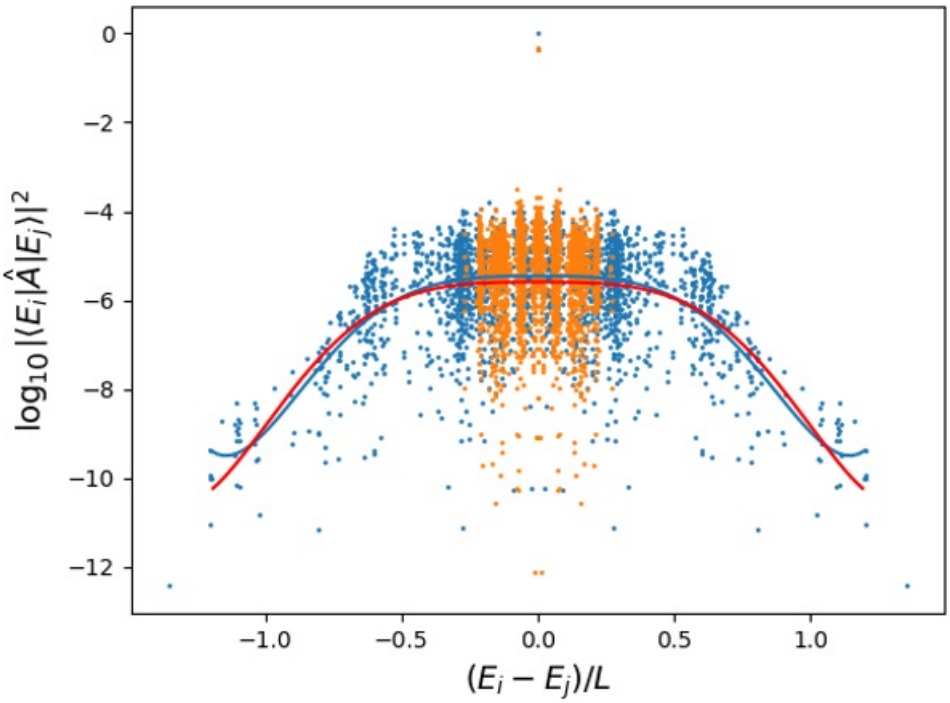

Figure 4.5: Matrix elements $|A_{ij}|^2$ within the energy band $\bar{E}_{\mathrm{QMBS}} = 0.1$ and width $\delta\bar{E}_{\mathrm{QMBS}} = 0.002$, Hamiltonian parameters $\{m, J, h, D, J_3, L\} = \{0, 1, 0, 0.1, 0.1, 10\}$, filter based on overlaps greater than $10^{-3.5}$ with AQMBS $|n, k\rangle$ with $n = L/2$, $k = \pi - \frac{2\pi}{L}$ (orange points) and with the staggered state $|+-\ldots+-\rangle$ (blue points).

1. the curve-fitting results (red line) for the points filtered based on the staggered state $|+-+-\ldots+-\rangle$ (represented by blue points) appear to be compatible with the line derived from the complete set of "average" matrix elements depicted in Fig. 4.4 (represented by the blue line).

2. On the other hand, the points filtered using the AQMBS state $|n, k\rangle$ (depicted as orange points) display a different behaviour. They exhibit a higher degree of localization around the diagonal matrix elements of the observable, and this subset of data does not reconstruct the curve observed in Fig. 4.4. We emphasize that the absence of outliers in the filtered distribution underscores our assertion that there are no explicit violations of the off-diagonal components of the ETH, at least in this context.

In conclusion, the analysis of the function $f(\bar{E}, \omega)$ following the implementation of a filtering procedure, which retains exclusively off-diagonal points correspond-

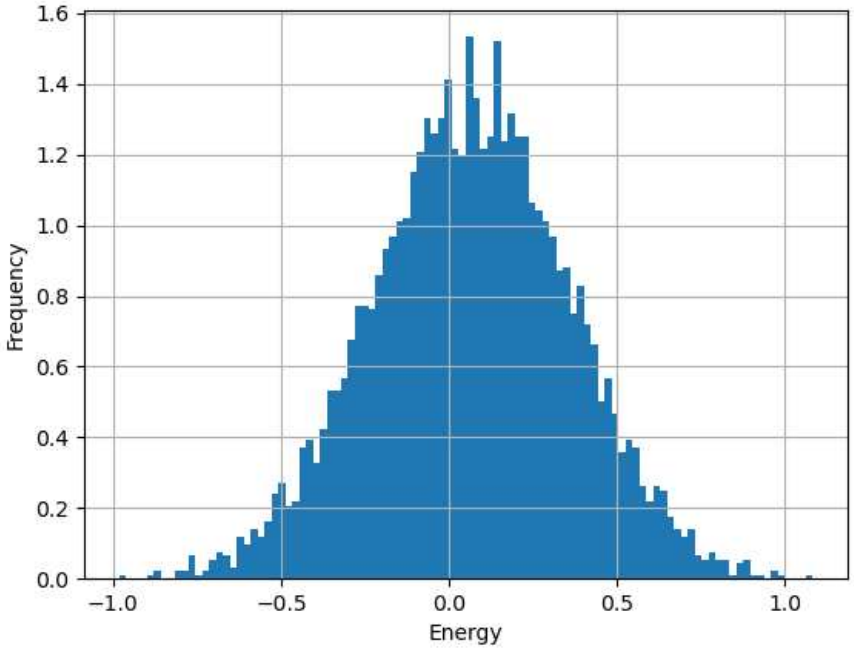

Figure 4.6: Energy density of states in the spatial inversion sector $I_\lambda = -1$. Hamiltonian parameters:$\{m, J, h, D, J_3, L\} = \{0, 1, 0, 0.1, 0.1, 10\}$.

ing to eigenstates showcasing substantial overlaps with the specifically considered state, introduces a novel method for discerning whether a particular state adheres to "thermal" behavior (conforming to the aggregate traits of the entire ensemble of states) or, conversely, corresponds to an AQMBS state.
Of fundamental importance is to acknowledge that the method outlined herein is inherently reliant on the specific state under consideration, a trait that warrants in-depth investigation in future research endeavours. Thus far, our inquiry has encompassed the analysis of various "thermal" states; nonetheless, it is noteworthy that the observed localization of data points around the diagonal matrix elements following the filtering process using an AQMBS is a novel observation. This finding imparts valuable insight and serves as a catalyst for further exploration in this research trajectory.

In conclusion, we have identified a well-defined function, denoted as f, which serves as a valuable criterion for discerning the "thermal" or non-thermal nature of a state. Furthermore, our findings indicate that the utilization of AQMBS primarily samples a specific segment of the energy spectrum and does not inherently

exhibit outliers in terms of the distribution of off-diagonal matrix elements. This observation, in turn, allows us to assert that explicit violations of the off-diagonal aspects of the ETH are not manifest in this context.

4.4 Off-diagonal matrix elements and energy density of states

In this brief section, we diverge slightly from the main discussion, yet our aim is to underscore the presence of a semi-periodic structure concealed within the distribution of off-diagonal matrix elements.
In Sec. 4.3, as depicted in Figure 4.4, we conducted an examination of the off-diagonal matrix element distribution. Specifically, we observed the presence of a plateau in the vicinity of the diagonal matrix elements and discerned different behavior at the edge of the spectrum. Upon a deeper analysis, it come up that the point distribution exhibits a semi-periodic structure, characterized by peaks that oscillate within the distribution.
In light of this observation, we resolved to investigate the energy density of states. As illustrated in Figure 4.6, this distribution in the spatial inversion sector $I_\lambda = -1$, also exhibits pronounced peaks, with a particular presence of three distinct peaks situated within the middle segment of the spectrum. However, it is essential to note that we do not possess complete knowledge of these phenomena, and further investigation is warranted.

Chapter 5

Construction of slow dynamics state

Until now, our discourse has revolved around the defining attributes of AQMBS, specifically their small energy variance and a limited amount of entanglement entropy. These distinctive traits facilitate the establishment of a relationship with the spectral properties of a local observable. Conversely, within this framework, we have not encountered any violation of the ETH, particularly about the off-diagonal component of the ETH, which plays a pivotal role in the system's long-term dynamics.
Hence, it may become imperative to both theoretically and experimentally engineer states that manifest comparable properties to those of AQMBS. Notably, this undertaking may start by considering "thermal" states, which typically occupy a more prominent presence within an energy spectrum when contrasted with AQMBS. Additionally, this approach could yield a deeper comprehension of AQMBS states within the framework of statistical mechanics, since we are approximating them with states that thermalize in the standard manner and thus well-described by the statistical mechanics. Subsequently, these artificially generated states can serve as a foundation for unveiling novel physical phenomena and furthering our comprehension of the underlying principles.

In this chapter, we introduce a numerical method for the generation of states that exhibit similar characteristics to those of AQMBS. Our approach starts with a brief analytical justification, highlighting the feasibility, particularly in the thermodynamic limit, of crafting states, with the asked features, derived from a pure state. These derived states are characterized by a small energy variance while concurrently allowing for controlled manipulation of the level of entanglement entropy employed. We clarify that this introductory analytical section serves solely as a means to introduce the conceptual framework that we intend to implement numerically. Our primary objective does not encompass a comparative evaluation of the results yielded by the analytical calculations. Therefore, at the end of the chapter,

we present numerical findings that serve as an initial foundation for subsequent research endeavours.

5.1 Theoretical framework

In Ref. [66], the authors have undertaken an investigation aimed at establishing a correlation between the energy variance and the entanglement entropy within a specific pure state. Their approach involved the introduction of a systematic method that initiates from a product state and subsequently constructs states characterized by decreasing energy variance, all while maintaining precise control over the degree of entanglement. This method was designed to be applicable to any local one-dimensional Hamiltonian.

We start by introducing the energy variance for a pure state $|\psi\rangle$ as follows:

$$\Delta H^2 \equiv \delta^2 = \langle\psi|\hat{H}^2|\psi\rangle - \langle\psi|\hat{H}|\psi\rangle^2. \tag{5.1}$$

This expression pertains to a spin chain with a local dimension of d and a local Hamiltonian $\hat{H}$ that can be represented as the summation of local operators $\hat{h}_i$. Notably, each of these operators $\hat{h}_i$ acts on adjacent spins, specifically, spin i and spin $i+1$.

To investigate the entanglement within a state, it is possible to introduce a "cut" at the i-th link of the chain, where $i \in \{1, \ldots, N-1\}$. This action effectively divides the chain into two distinct regions, each characterized by its number of spins: i spins in one region and $(N-i)$ spins in the other. The entanglement entropy, concerning this particular partition, is formally defined as:

$$S_i = -\mathrm{Tr}(\hat{\rho}_i \log_2 \hat{\rho}_i) = S_{N-i}, \tag{5.2}$$

where the reduced state $\hat{\rho}_i = \mathrm{Tr}_{i+1,\ldots,N}|\psi\rangle\langle\psi|$.

We consider entangled states of the form

$$|\psi\rangle = \frac{1}{\mathcal{N}} \sum_{m=-\infty}^{+\infty} c_m e^{i2m\hat{H}/N}|p\rangle, \tag{5.3}$$

where $|p\rangle$ is a product state with energy $E_p = \langle p|\hat{H}|p\rangle = 0$, variance $\sigma_p = \frac{a}{\sqrt{N}}$ with $a = \mathcal{O}(1)$, and $\mathcal{N}$ is the normalization factor.

They applied an operator such that the variance of the resulting state $|\psi\rangle$ systematically decreases in the number of terms in the sum. In particular, let the following operator:

$$\left[\cos\frac{\hat{H}}{N}\right]^M = \frac{1}{2^M} \sum_{m=-M/2}^{M/2} \binom{M}{M/2-m} e^{i2m\hat{H}/N}. \tag{5.4}$$

The operator's effect on the state $|p\rangle$ can be represented using Eq. (5.3), with $-x\sqrt{M} \leq m \leq x\sqrt{M}$ terms, $x = \mathcal{O}(1)$, thereby reducing the energy variance of the resulting state. Importantly, we stress that for values of $|X|$ where $|X| < 1$, the expression $\cos^M(X)$ can be approximated as $e^{-MX^2/2}$. This approximation is particularly relevant for our numerical calculations, where the exponential operator plays a pivotal role.
Specially, from the application of the operator in Eq. (5.4) the resulting state's variance is then determined for sufficiently large systems, it scales as [77]:

$$\delta = \sqrt{\frac{N}{2M}}. \tag{5.5}$$

It is important to note that the entanglement of any state conforming to the structure described by Eq. (5.3) can be bounded from above by a function dependent on the bond-dimension D associated with the corresponding Matrix Product State (MPS) representation of the state. Utilizing results from Ref. [66, 78–82] about limiting the bond-dimension D, thus the amount of entanglement entropy since it holds

$$S \approx \log(D), \tag{5.6}$$

in the thermodynamic limit, we recover that

$$S \leq \log_2 \frac{k_1}{\delta} + \frac{1}{2}\log_2 N + k_2, \tag{5.7}$$

where k_1 and k_2 are constants of order $\mathcal{O}(1)$. This analysis reveals the possibility of constructing states with small energy variance and sub-extensive entanglement entropy, features that characterize AQMBS states, from product states.

5.2 Numerical study

Building upon the discussion in the previous section, we advance towards the implementation of a Gaussian filter applied to a general quantum pure state $|\psi\rangle$. This state is not necessarily an eigenstate of the Hamiltonian specified in Eq. (3.1), and notably, we have established the condition $J_3 = 0$.
Within this framework, we adhere to the following sequential procedure:

1. We commence by subjecting the quantum state $|\psi\rangle$ to the operator $e^{-\tau\left(\hat{H}-E_0\right)^2}$, where $\tau \in \mathbb{C}$, and E_0 represents the energy associated with the QMBS $|n, \pi\rangle$ of the model.

2. We calculate the energy variance ΔH^2 and the bipartition entanglement entropy $s(E_i) = -\frac{2}{L}\mathrm{Tr}[\hat{\rho}_{A,E_i} \log \hat{\rho}_{A,E_i}]$ (as discussed in Chap. 3) of the evolved state, before appropriate normalization.

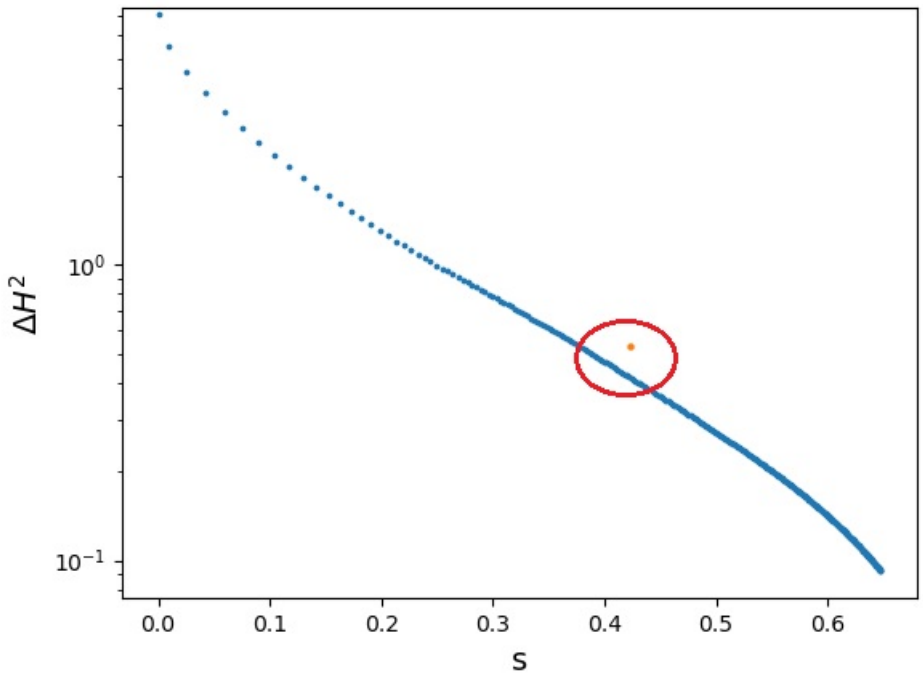

Figure 5.1: Evolution of the energy variance ΔH^2 and the bipartition entanglement entropy s using the Gaussian filter algorithm. The initial state is $|+-\ldots+-\rangle$, and the model corresponds to the Hamiltonian in Eq. (3.1) with parameters $\{m, J, h, D, J_3, L\} = \{0, 1, 0, 0.1, 0, 8\}$. The orange point, highlighted by the red circle, represents the AQMBS $|n, k\rangle$ state with $n = L/2$ and $k = \pi - \frac{2\pi}{L}$. The values were computed using exact diagonalization.

3. The procedure is then iteratively repeated by applying the exponential operator once again to the evolved state.

The outlined procedure undoubtedly leads to the creation of states characterized by reduced variance in energy and a sub-extensive degree of entanglement entropy. However, we stress that these criteria alone may not guarantee that the resulting states exhibit the salient features of AQMBS.
Specifically, while our procedure may generate states with sub-extensive entanglement entropy, it remains possible that the magnitude of this entropy is not sufficiently small to be directly comparable with well-established AQMBS states. The presence of sub-extensive entanglement alone may not guarantee the unique characteristics associated with AQMBS.
Therefore, it is important to employ additional measures to rigorously determine whether the states produced through this procedure indeed exhibit the defining

properties of AQMBS.

In our investigation, we employed the numerical technique of exact diagonalization. As our starting point, we adopted the usual staggered state, denoted as $|\psi\rangle = |+-+-\ldots+-\rangle$. Subsequently, we executed the algorithm outlined in the previous sections.
As depicted in Fig. 5.1, the alignment of our evolving state with AQMBS characteristics becomes increasingly pronounced as the algorithm progresses. This observation underscores the effectiveness of our approach in generating states that exhibit behaviors and properties akin to AQMBS states.
Despite the valuable insights gained through exact diagonalization, it is essential to recognize that this method does not provide conclusive information regarding the behavior of systems in the thermodynamic limit ($L \to \infty$), where experimental comparisons become feasible. To address this, we turned to tensor network methods, specifically leveraging the Time Dependent Variational Principle (TDVP) [83–86]. It is important to acknowledge that our mastery of this approach is not yet comprehensive, which implies that we refrain from making definitive inferences concerning the behavior of our states in comparison with AQMBS states.

It is crucial to acknowledge that our utilization of the aforementioned tensor network method is not in our full control. Consequently, to date, we are not able to draw definitive conclusions regarding the behavior of our states when compared to AQMBS states. Nevertheless, it is paramount to highlight that, despite these methodological challenges, our endeavors have yielded noteworthy accomplishments. In particular, we have successfully created quantum states that exhibit distinctive characteristics, including minimal energy variance and a restricted level of entanglement entropy, particularly within the thermodynamic limit.
Furthermore, our research endeavors have encompassed the execution of numerical simulations encompassing significant chain sizes, extending to systems containing up to 100 particles. Our objective in these simulations is to investigate and analyze the behavior of the generated quantum states while systematically varying the system size denoted by L. As elucidated in Fig. 5.2, we have conducted a comparative analysis of the state's behavior under varying system sizes. Specifically, we have examined the relationship between the intensive energy variance ΔH^2 and the extensive entanglement entropy. Notably, our findings reveal a qualitatively correlation between these two key properties, which provides a valuable foundation for future explorations and investigations.

In summary, our research endeavors have led to the creation of quantum states derived from an initial "thermal" state. These newly constructed states exhibit noteworthy characteristics that are comparable to those of AQMBS, particularly evident when considering smaller system sizes denoted as L. Furthermore, we have

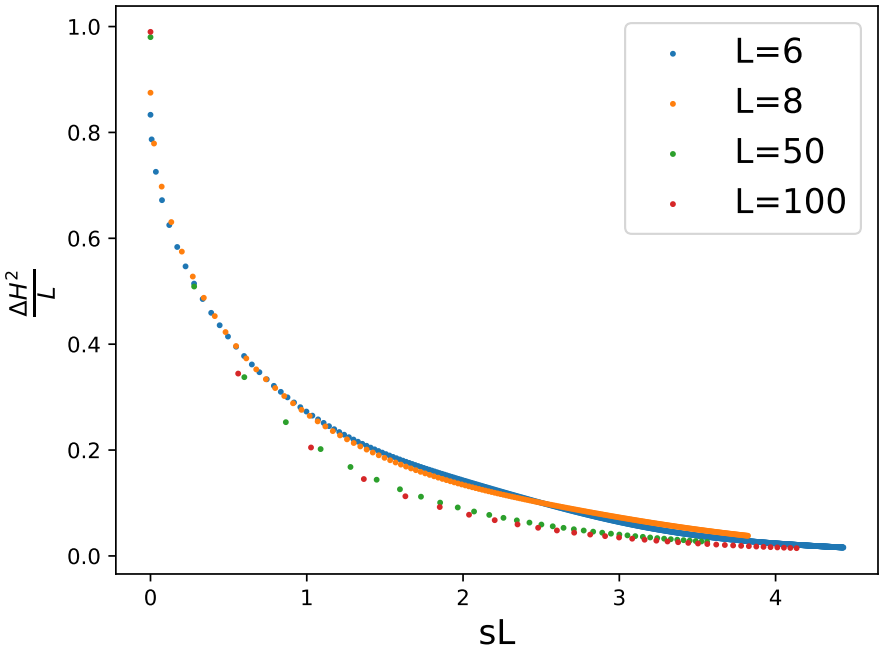

Figure 5.2: Comparison of the TDVP evolution at different L. The initial "thermal" state is $|+-\ldots+-\rangle$. Hamiltonian parameters: $\{m, J, h, D, J_3\} = \{0, 1, 0, 0.1, 0.1, 0\}$.

embarked on the exploration of the thermodynamic limit ($L \to \infty$). At present, drawing definitive conclusions in this context remains challenging. Nevertheless, the observed correlation, as highlighted, between the state's properties, such as intensive energy variance and extensive entanglement entropy, serves as a promising point of departure for future investigations and studies.

Conclusions

This thesis has delved into the realm of thermalization, a concept that has fascinated scientists for centuries as they seek to bridge the gap between macroscopic behaviour and microscopic dynamics. While statistical mechanics has successfully described the macroscopic properties of systems, the profound link between these properties and microscopic interactions continues to be a subject of exploration and discussion.

In this research, our initial focus centres on the review and the discussion of the behaviour of quantum systems, particularly highlighting the distinctions and disparities between quantum systems and their classical counterparts. The analogy of a coloured drop diffusing within a liquid introduced us to the concept of thermalization in classical systems and prompted the question of whether quantum systems exhibit similar behaviour.

The recent and significant advancement embodied by the Eigenstate Thermalization Hypothesis (ETH) has introduced a robust and comprehensive framework for comprehending the phenomenon of thermalization in quantum systems. This framework unites concepts of chaos and ergodicity within a distinctive mathematical formulation. The ETH, as systematically defined in Chap. 1, constitutes a statistical statement that elucidates the behaviour of observables, particularly their convergence towards equilibrium conditions in chaotic quantum systems. Nonetheless, the emergence of exceptional states that overtly contravene the diagonal aspect of the ETH has given rise to a novel realm of inquiry known as quantum many-body scars (QMBS). These particular states are Hamiltonian eigenstates. They typically occupy a position within the middle segment of the spectrum of eigenstates. What sets QMBS different is their distinctive behaviour with regard to entanglement entropy when compared to other states residing within the same energy shell. The entanglement entropy exhibited by QMBS states stands out as anomalous or unique in contrast to its counterparts, rendering them a distinctive class of quantum states within the spectrum. Therefore, these QMBS challenge traditional conceptions of thermalization by unveiling distinct manifestations of non-thermal behaviour within observables.

Recent research findings, as documented in Ref. [10], have extended the con-

cept of quantum many-body scars to encompass a broader category referred to as asymptotic quantum many-body scar states (AQMBS). AQMBS states are conjectured to play a pivotal role in the violation of the off-diagonal aspect of the ETH due to their primary characteristic: slow relaxation dynamics towards equilibrium conditions.

In Chap. 4, we have undertaken a comprehensive investigation of the AQMBS states present in a spin-1 XY chain. Our primary focus was to explore their behaviour about the violation of the off-diagonal elements of the ETH. Specifically, we examined the connection between the function f defined in ETH, thus the spectral properties of observables, with the slow dynamics that AQMBS presents. We have successfully identified and characterized a well-defined function f, which can be used as a valuable criterion for making clear distinctions between the "thermal" and non-thermal attributes of a quantum state. Our research findings substantiate that the utilization of AQMBS predominantly targets a specific sector within the energy spectrum, bringing us to a very different function f with respect to what we would obtain if we analyse "thermal" states. Moreover, the selection does not inherently introduce outliers or anomalies in the distribution of off-diagonal matrix elements. Consequently, based on our observations, we can confidently assert that explicit violations of the off-diagonal aspects of the ETH are not manifest in the context of AQMBS states.

In Chap. 5, we have devised a systematic procedure for the generation of quantum states that exhibit similar properties of the AQMBS. This approach starts with an initial "thermal" state and subsequently transforms it into states bringing the distinctive characteristics associated with AQMBS. The achievement, at least for small systems, of generating AQMBS-like states through this procedure opens up avenues for more extensive investigations. These investigations may lead to the revelation of additional and hitherto undiscovered characteristics and properties inherent to AQMBS states, thereby enriching our comprehension of these remarkable quantum states. Nonetheless, to match experiments with theoretical constructs, we need the capability to scrutinize physical systems in the thermodynamic limit. The progression of such an inquiry necessitates supplementary investigations, the study of which remains, as of the present, incompletely mastered.

The observations and discoveries elucidated within this thesis serve as a catalyst, inspiring and motivating further research endeavours and advancements aimed at deepening our comprehension of the behaviour exhibited by exceptional states within quantum many-body systems. Furthermore, we stress that the research journey embarked upon in this study has its roots in an experiment involving Rydberg atoms. This experimental endeavour represents one of the promising avenues towards the realization of quantum hardware, which is at the forefront of contemporary quantum technology development.

In conclusion, this study not only enriches our understanding of quantum phenomena but also offers tangible prospects for the practical implementation of quantum hardware, thereby contributing to the ongoing evolution of quantum science and technology.

Acknowledgments

G.M. extends heartfelt appreciation for the intellectually stimulating dialogues with Professors Luca Dell'Anna and Maurizio Fagotti throughout the course of this research endeavour. Gratitude is also extended to colleague Brian Moglia for his contribution to the implementation of the Time-Dependent Variational Principle (TDVP) algorithm. Moreover, G.M. acknowledges the hospitality of the Laboratoire de Physique Théorique et Modèles Statistiques (LPTMS) in Orsay, where the collaboration with Professors Simone Montangero and Leonardo Mazza was initiated.

Bibliography

[1] L. D'Alessio et al. *From Quantum Chaos and Eigenstate Thermalization to Statistical Mechanics and Thermodynamics*. Advances in Physics, 2016. DOI: https://doi.org/10.1080/00018732.2016.1198134.

[2] W. Beugeling, R. Moessner, and M. Haque. Phys. Rev. E 89, (2014), p. 042112. DOI: https://doi.org/10.1103/PhysRevE.89.042112.

[3] R. Mondaini et al. Phys. Rev. E 93, (2016), p. 032104. DOI: https://doi.org/10.1103/PhysRevE.93.032104.

[4] C. Neuenhahn and F. Marquardt. Phys. Rev. E 85, (2012), p. 060101. DOI: https://doi.org/10.1103/PhysRevE.85.060101.

[5] M. Rigol, V. Dunjko, and M. Olshanii. Nature 452, (2008), p. 854. DOI: https://doi.org/10.1038/nature06838.

[6] L.F. Santos and M. Rigol. Phys. Rev. E 82, (2010), p. 031130. DOI: https://doi.org/10.1103/PhysRevE.82.031130.

[7] H. Bernien et al. In: *Nature* 551 (2017), pp. 579–584. DOI: https://doi.org/10.1038/nature24622.

[8] C. J. Turner et al. *Weak ergodicity breaking from quantum many-body scars*. Nature Physics, 14(7): 745-749, 2018. DOI: https://doi.org/10.1038/s41567-018-0137-5.

[9] A. Chandran et al. *Quantum Many-Body Scars: A Quasiparticle Perspective*. Annual Review of Condensed Matter Physics, 2022. DOI: https://doi.org/10.1146/annurev-conmatphys-031620-101617.

[10] L. Gotta, S. Moudgalya, and L. Mazza. *Asymptotic Quantum Many-Body Scars*. arXiv:2303.05407v1 [cond-mat. str-el], 2023. DOI: https://doi.org/10.48550/arXiv.2303.05407.

[11] P. Cvitanovic et al. *Chaos: Classical and Quantum*. ChaosBook.org, Niels Bohr Institute, Copenhagen, 2012. URL: https://chaosbook.org.

[12] M. C. Gutzwiller. *Chaos in Classical and Quantum Mechanics*. Springer New York, NY, 2013. DOI: https://doi.org/10.1007/978-1-4612-0983-6.

[13] A. Bäcker. *Quantum chaos in billiards*. Computing in Science & Engineering, 2007. DOI: https://doi.org/10.1109/MCSE.2007.61.

[14] G. Zaslavsky. *Physics of Chaos in Hamiltonian Systems*. 1998. URL: https://api.semanticscholar.org/CorpusID:115292925.

[15] J. V. José and E. J. Saletan. *Classical Dynamics: A Contemporary Approach*. Cambridge Univ. Press, 1998. DOI: https://doi.org/10.1017/CBO9780511803772.

[16] V.I. Arnold. *Mathematical Methods of Classical Mechanics*. Springer-Verlag, New York, 1989. DOI: https://doi.org/10.1007/978-1-4757-1693-1.

[17] H. Scott Dumas. *The KAM Story: A Friendly Introduction to the Content, History, and Significance of Classical KAM Theory*. World Scientific Publishing Company, 2014. DOI: https://doi.org/10.1142/8955.

[18] L. Correale et al. arXiv:2303.15393v1, 2023. DOI: https://doi.org/10.48550/arXiv.2303.15393.

[19] F. Haake. *Quantum Signatures of Chaos*. Springer-Verlag, New York, 1991. DOI: https://doi.org/10.1007/978-3-642-05428-0.

[20] D. Rossini and R. Fazio. *Quantum Information Processing and Quantum Spin Systems*. Scuola Normale Superiore Pisa, Ph.D. thesis, 2007. URL: https://ricerca.sns.it/retrieve/handle/11384/85856/37478/Rossini_Davide.pdf.

[21] E.P. Wigner. *Gatlinberg Conference on Neutron Physics*. Rep. ORNL-2309, p.57, 1957. URL: https://www.ornl.gov.

[22] O. Bohigas, M. J. Giannoni, and C. Schmit. *Characterization of Chaotic Quantum Spectra and Universality of Level Fluctuation Laws*. Phys. Rev. Lett. 52,1, 1984. DOI: https://doi.org/10.1103/PhysRevLett.52.1.

[23] J. S. Caux and J. Mossel. arXiv:1012.3587v1 [cond-mat.str-el], 2010. DOI: https://doi.org/10.1088/1742-5468/2011/02/P02023.

[24] J. Von Neumann. Zeitschrift für Physik, 1929. URL: https://www.epj.org/.

[25] S. Goldstein et al. European Phys. J. H 35, 2010. DOI: https://doi.org/10.1140/epjh/e2010-00007-7.

[26] J. M. Deutsch. Phys. Rev. A 43, 2046, 1991. DOI: https://doi.org/10.1103/PhysRevA.43.2046.

[27] M. Srednicki. Phys. Rev. E 50, 1994. DOI: https://doi.org/10.1103/PhysRevE.50.888.

[28] M. Srednicki. J. Phys. A 29, 1996. DOI: https://doi.org/10.1088/0305-4470/29/4/003.

[29] M. Srednicki. J. Phys. A 32, 1999. DOI: https://doi.org/10.1088/0305-4470/32/7/007.

[30] M. Rigol, V. Dunjko, and M. Olshanii. Nature 452, 2008. DOI: https://doi.org/10.1038/nature06838.

[31] M. Rigol and M. Srednicki. Phys. Rev. Lett. 108, 110601, 2012. DOI: https://doi.org/10.1103/PhysRevLett.108.110601.

[32] B. Craps et al. arXiv:2305.00037v2, 2023. DOI: https://doi.org/10.48550/arXiv.2305.00037.

[33] A. Chandran et al. *Quantum Many-Body Scars: A Quasiparticle Perspective*. Annual Review of Condensed Matter Physics, 2022. DOI: https://doi.org/10.1146/annurev-conmatphys-031620-101617.

[34] C. J. Turner et al. Phys. Rev. X 11, 021021, 2021. DOI: https://doi.org/10.1103/PhysRevX.11.021021.

[35] W. W. Ho et al. Phys. Rev. Lett. 122, 040603, 2019. DOI: https://doi.org/10.1103/PhysRevLett.122.040603.

[36] S. DOoley. PRX Quantum 2, 020330, 2021. DOI: https://doi.org/10.1103/PRXQuantum.2.020330.

[37] J. Y. Desaules et al. Phys. Rev. Lett. 129, 020601, 2022. DOI: https://doi.org/10.1103/PhysRevLett.129.020601.

[38] A. A. Michailidis et al. Phys. Rev. Research 2, 022065(R), 2020. DOI: https://doi.org/10.1103/PhysRevResearch.2.022065.

[39] A. A. Michailidis et al. Phys. Rev. X 10, 011055, 2020. DOI: https://doi.org/10.1103/PhysRevX.10.011055.

[40] S. Moudgalya, B. A. Bernevig, and N. Regnault. *Quantum Many-Body Scars and Hilbert Space Fragmentation: A Review of Exact Results*. Rep. Prog. Phys. 85 086501, 2022. DOI: https://doi.org/10.1088/1361-6633/ac73a0.

[41] D. Bluvstein et al. In: *Science* 371 (2021), pp. 1355–1359. DOI: https://doi.org/10.1126/science.abg2530.

[42] P. Sala et al. Phys. Rev. X 10(1) 011047, 2020. DOI: https://doi.org/10.1103/PhysRevX.10.011047.

[43] N. Shiraishi and T. Mori. Phys. Rev. Lett. 119(3) 030601, 2017. DOI: https://doi.org/10.1103/PhysRevLett.119.030601.

[44] D. K. Mark, C. J. Lin, and O. I. Motrunich. Phys. Rev. B 101(19) 195131, 2020. DOI: https://doi.org/10.1103/PhysRevB.101.195131.

[45] S. Moudgalya, N. Regnault, and B. A. Bernevig. Phys. Rev. B 102(8) 085140, 2020. DOI: https://doi.org/10.1103/PhysRevB.101.094308.

[46] K. Pakrouski et al. Phys. Rev. Lett. 125(23) 230602, 2020. DOI: https://doi.org/10.1103/PhysRevLett.125.230602.

[47] J. Ren, C. Liang, and C. Fang. Phys. Rev. Lett. 126(12) 120604, 2021. DOI: https://doi.org/10.1103/PhysRevLett.126.120604.

[48] N. O'Dea et al. Phys. Rev. Research 2(4) 043305, 2020. DOI: https://doi.org/10.1103/PhysRevResearch.2.043305.

[49] M. Schecter and T. Iadecola. *Weak ergodicity breaking and quantum many-body scars in spin-1 xy magnets*. Phys. Rev. Lett. 123(14) 147201, 2019. DOI: https://doi.org/10.1103/PhysRevLett.123.147201.

[50] D. K. Mark and O. I. Motrunich. Phys. Rev. B 102(7) 075132, 2020. DOI: https://doi.org/10.1103/PhysRevB.102.075132.

[51] S. Choi et al. Physical Review Letters 122(22) 220603, 2019. DOI: https://doi.org/10.1103/PhysRevLett.122.220603.

[52] C. N. Yang. Phys. Rev. Lett. 63, 2144, 1989. DOI: https://doi.org/10.1103/PhysRevLett.63.2144.

[53] C. N. Yang and S. C. Zhang. Modern Physics Letters B 4, 1990. DOI: https://doi.org/10.1142/S0217984990000933.

[54] F. H. Essler et al. *The one-dimensional Hubbard model*. Cambridge University Press, 2005. DOI: https://doi.org/10.1017/CBO9780511534843.

[55] O. Vafek, N. Regnault, and B. A. Bernevig. SciPost Phys. 3(6) 043, 2017. DOI: https://doi.org/10.21468/SciPostPhys.3.6.043.

[56] R. Mondaini et al. Phys. Rev. Lett. 121(3) 038901, 2018. DOI: https://doi.org/10.1103/PhysRevLett.121.038901.

[57] V. Khemani, M. Hermele, and R. Nandkishore. Phys. Rev. B 101(17) 174204, 2020. DOI: https://doi.org/10.1103/PhysRevB.101.174204.

[58] S. Moudgalya and O. I. Motrunich. Phys. Rev. X 12(1) 011050, arXiv:2108.10324, 2022. DOI: https://doi.org/10.1103/PhysRevX.12.011050.

[59] A. Kitazawa, K. Hijii, and K. Nomura. J. Phys. A 36, L351, 2003. DOI: https://doi.org/10.1088/0305-4470/36/23/104.

[60] Y. Y. Atas et al. *The distribution of the ratio of consecutive level spacings in random matrix ensembles*. Phys. Rev. Lett. 110, 084101, 2013. DOI: https://doi.org/10.1103/PhysRevLett.110.084101.

[61] M. L. Mehta. *Random Matrix Theory*. Elsevier/Academic Press, 2004. URL: https://books.google.it/books?id=QWOYjgEACAAJ.

[62] G. Biroli, C. Kollath, and A. M. Läuchli. Phys. Rev. Lett. 105, 250401, 2010. DOI: https://doi.org/10.1103/PhysRevLett.105.250401.

[63] Page. Don N. *Average entropy of a subsystem.* Phys. Rev. Lett., 71, 1993. DOI: https://doi.org/10.1103/PhysRevLett.71.1291.

[64] L. H. Tang, N. O'Dea, and A. Chandran. Phys. Rev. Res. 4, 043006, 2022. DOI: https://doi.org/10.1103/PhysRevResearch.4.043006.

[65] S. Moudgalya, N. Regnault, and B. A. Bernevig. Phys. Rev. B 98, 235156, 2018. DOI: https://doi.org/10.1103/PhysRevB.98.235156.

[66] M. C. Bañuls, D. A. Huse, and J. I. Cirac. Phys. Rev. B 101, 144305, 2020. DOI: https://doi.org/10.1103/PhysRevB.101.144305.

[67] H. Wilming et al. Springer, Cham, 2019. DOI: https://doi.org/10.1007/978-3-319-99046-0_18.

[68] T. Mori et al. Journal of Physics B: Atomic, Molecular and Optical Physics 51, 112001, 2018. DOI: https://doi.org/10.1088/1361-6455/aabcdf.

[69] S. Goldstein, T. Hara, and H. Tasaki. Phys. Rev. Lett. 111, 140401, 2013. DOI: https://doi.org/10.1103/PhysRevLett.111.140401.

[70] A. S. L. Malabarba et al. Phys. Rev. E 90, 012121, 2014. DOI: https://doi.org/10.1103/PhysRevE.90.012121.

[71] S. Goldstein, T. Hara, and H. Tasaki. Journal of Physics 17, 045002, 2015. DOI: https://doi.org/10.1088/1367-2630/17/4/045002.

[72] P. Reimann. Nature Communications 7, 10821, 2016. DOI: https://doi.org/10.1038/ncomms10821.

[73] L. P. García-Pintos et al. Phys. Rev. X 7, 031027, 2017. DOI: https://doi.org/10.1103/PhysRevX.7.031027.

[74] J. Riddell, L. P. García-Pintos, and A. M. Alhambra. arXiv:2112.09475, 2021. DOI: https://doi.org/10.48550/arXiv.2112.09475.

[75] C.-J. Lin, A. Chandran, and O. I. Motrunich. Phys. Rev. Res. 2, 033044, 2020. DOI: https://doi.org/10.1103/PhysRevResearch.2.033044.

[76] N. Shiraishi and T. Mori. Phys. Rev. Lett. 121, 038902, 2018. DOI: https://doi.org/10.1103/PhysRevLett.121.038902.

[77] F. Verstraete, V. Murg, and J. I. Cirac. Adv. Phys. 57, 143, 2008. DOI: https://doi.org/10.1080/14789940801912366.

[78] M. Hartmann, G. Mahler, and O. Hess. Lett. Math. Phys. 68, 103, 2004. DOI: https://doi.org/10.1023/B:MATH.0000043321.00896.86.

[79] W. Dür et al. Phys. Rev. Lett. 87, 137901, 2001. DOI: https://doi.org/10.1103/PhysRevLett.87.137901.

[80] C. H. Bennett et al. IEEE Trans. Inf. Theory 49, 2003. DOI: https://doi.org/10.1109/TIT.2003.814935.

[81] S. Bravyi. Phys. Rev. A 76, 052319, 2007. DOI: https://doi.org/10.1103/PhysRevA.76.052319.

[82] K. Van Acoleyen, M. Mariën, and F. Verstraete. Phys. Rev. Lett. 111, 170501, 2013. DOI: https://doi.org/10.1103/PhysRevLett.111.170501.

[83] S. Montangero. *Introduction to Tensor Network Methods*. Springer, Cham, 2018. DOI: https://doi.org/10.1007/978-3-030-01409-4.

[84] T. Paeckel S.and Köhlera et al. *Time-evolution methods for matrix-product states*. Annals of Physics 411, 167998, 2019. DOI: https://doi.org/10.1016/j.aop.2019.167998.

[85] J. Haegeman et al. *Time-dependent variational principle for quantum lattices*. Phys. Rev. Lett. 107, 070601, 2011. DOI: https://doi.org/10.1103/PhysRevLett.107.070601.

[86] C. Lubich, I. Oseledets, and B. Vandereycken. *Time integration of tensor trains*. SIAM Journal on Numerical Analysis, 2015. DOI: https://doi.org/10.1137/140976546.